Marcus Takvam Lexander

Response Theory Based Methods for Electronic Transport

Master's thesis in Applied Theoretical Chemistry
Supervisor: Ida-Marie Høyvik
September 2021

Master's thesis

NTNU
Norwegian University of Science and Technology
Faculty of Natural Sciences
Department of Chemistry

NTNU
Norwegian University of
Science and Technology

Marcus Takvam Lexander

Response Theory Based Methods for Electronic Transport

Master's thesis in Applied Theoretical Chemistry
Supervisor: Ida-Marie Høyvik
September 2021

Norwegian University of Science and Technology
Faculty of Natural Sciences
Department of Chemistry

NTNU
Norwegian University of
Science and Technology

Sammendrag

Nanoelektronikk er er fagfelt som blir mer og mer relevant nå som elektronikk blir mindre og raskere, og med rask utvikling av teknologier som superledere og kvantedatamaskiner. Dette er et forskningsfelt der det har vært mye fremgang i mange tiår. Denne fremgangen ser ikke ut til å stoppe. Et spesifikt område der det forsatt er stor utvikling er kvantemekanisk optoelektronikk, hvor vi ser på interaksjonen mellom lys og molekylære ledere, som det transporteres elektroner gjennom. Det finnes enda ikke et godt rammeverk for å teoretisk modellere denne interaksjonen. I denne avhandlingen introduserer vi en metode basert på lineær responsteori, et rammeverk hvor det å beskrive optiske egenskaper til molekyler er vanlig, for å beskrive elektronisk transport mellom forskjellige deler av et lukket molekylært system. Med dette gir vi noen enkle proof-of-concept beregninger for to enkle molekyler, ett hvor vi ser på transporten mellom et hydrogenatom og et litiumatom, og ett annet hvor vi ser på transport mellom et berylliumatom og et oksygenmolekyl. Disse beregningene er basert på modelperturbasjoner som ikke vil representere kvantitativt nøyaktige forutsigelser, men heller er gjort for å vise potensialet for videreutviklingen av en slik metode for å gi en god beskrivelse av like transportfenomener. For noen former av slike perturbasjoner har vi observert en forflytning på rundt 0.9 elektroner per perturbasjonsstyrke på 1 a.u. Dette har blitt gjort sammen med en beregning av elektrisk strøm gjennom et modellsystem av tre hydrogenmolekyl under en påført spenning, ved å bruke en ikke-likevekts Greens funksjonsmetode (Non-Equlibrium Green's Function, NEGF), som er en av de fundamentale metodene for å beskrive kvantemekanisk transport. Dette er gjort for å ha en lignende beregning for å kunne sammenligne responseteorimetoden med, både den interne matematikken av de to metodene, og de beregnede resultatene. Likevel, siden responseteorimetoden ikke enda inkluderer en beskrivelse av kontakter til elektronreservoarer som er essensielt for å ha kontinuerlig strøm. Derfor kan vi ikke direkte sammenligne resultatene fra disse to metodene, som vi kunne ha gjort dersom metodene beregnet samme størrelse.

Abstract

The field of nanoelectronics is becoming increasingly relevant as electronics become smaller and faster and with the rapid development in technologies such as superconductors and quantum computers. This is a field that has seen a lot of progress for the last many decades and continues to do so. One particular area that is still seeing a lot of development is quantum optoelectronics, where we look at the interaction between light and molecular conducting channels undergoing electronic transport. There does not yet exist a rigorous framework for theoretically modeling this interaction properly. In this thesis we introduce a method based on linear response theory, a framework where describing optical properties of molecules is commonplace, for describing electronic transport between different parts of a closed molecular system. With this, we provide some simple proof-of-concept calculations for two simple molecules, one where we calculate the transport of electrons between a hydrogen and lithium atom, and the other calculating transport between a beryllium atom and an oxygen molecule. These calculations are based on model perturbations that will not represent quantitatively accurate predictions, but rather serves to show the potential of the method to be further developed for a good description of such transport phenomena. For certain types of perturbations, we observed a movement of the electronic density corresponding to about 0.9 electrons per perturbation strength of 1 a.u. This has been done alongside a calculation of the steady state current through a model system consisting of three hydrogen molecules under a potential bias, using the Non-Equilibrium Green's Function (NEGF) method, which is one of the fundamental pillars of describing quantum transport. This is done to have a similar calculation to compare the response theory method to, both in terms of the internal mathematics of the two methods, and the predicted results. However, the response theory method does not yet include a description of contacts to external electron reservoirs, which is required for steady state transport. As such, the results from the two methods is not as directly comparable as if they both calculated the same quantity.

Preface

This thesis was performed and submitted to the "Norwegian University of Science and Technology" (NTNU), Department of Chemistry, and concludes the master's degree programme in Chemistry (MSCHEM) with specialization in applied theoretical chemistry. The present work was carried out between August 2020 and September 2021, supervised by Prof. Ida-Marie Høyvik.

Acknowledgements

I would like to give a special thanks to my supervisor Ida-Marie Høyvik. A short acknowledgement like this has no chance of showing the appreciation I have for all she has done for me. Without her energy, enthusiasm, motivation and intellect, I would never have made it through this immense task. All of the time she has taken to discuss and help develop the theory, as well as motivate me, has made the last year both a fun and rewarding experience. The amount of excellent quality feedback and criticism, especially in the final stretch, has helped me keep motivation and improved my productivity and the quality of my work by several orders of magnitude.

I also would like to thank all my friends and family that have helped keep morale and motivation up through the last year. A special thanks goes out to Sverre Emanual Dårflot Olsen, Bjørnar Ørjansen Kaarevik and Ylva Os for having put up with listening to and discussing much of the material that has ended up in the thesis, as well as helping with proofreading the final version.

Contents

Chapter 1

Introduction

Electronic transport at the nanoscale is an important field of research which has seen a lot of development, both experimentally and theoretically for the last few decades. Consumer-grade microelectronics have reached the point of having a manufacturing node of 5nm[1, 2], roughly relating to the size of the active region of transistors. This is only about 40 silicon atoms and the research and development is happening for even smaller scales[3, 4]. Working at this scale, a good theoretical description of electronic transport is essential. A lot of models have been made and used over the years, using both empirical and *ab-initio* approaches[5, 6]. Many of these methods have shown great success for describing certain phenomena[7], but there are a lot of areas which still need a lot of research[8]. A well studied system is the molecular junction, in which a single molecule is placed between and coupled to some, usually two, electrodes, usually made of some gold or semiconductor material. There have been a lot of both theoretical[7, 8] and experimental[9, 10] studies into various properties of these molecular junctions, with theoretical calculations of the characteristics of a single molecule rectifier going back to the 1970s[7]. This includes electrical[9], mechanical[11], thermoelectric[12] and optical[13] properties as well as other quantum properties like Coulomb, Frank-Condon and spin blockades[14–16], interference/decoherence[17, 18] and much more. The field of molecular optoelectronics, which concerns itself with the interaction between such molecular junctions and light, is a rapidly expanding field, with many important applications such as light controlled switches[10, 13, 19] and transistors[14], that can be used for electronic components as photonic memory devices[20]. However, no current theory of transport exists which treat the electronic structure of the system explicitly in a framework where accurately predicting optical properties is possible. Having such a theory would enable the theoretical modeling of many phenomena in molecular junctions that is not currently possible.

Another system where the interaction between light and molecules undergoing electronic transport is photoredox catalysis[21–24], where light is used to initiate otherwise energetically difficult reactions. A classic example of this in nature is photosynthesis, in which sunlight is catalysing the construction of sugar from the very energetically stable raw materials, carbon dioxide and water. A good theoretical description of such photo-activated processes would further enable the development and testing of photoredox catalysis methods for synthesising

various organic substances that might otherwise need expensive, dangerous, or environmentally hurtful chemicals to make.

1.1   Current Descriptions of Transport

Theoretical descriptions of macroscopic transport have been well understood for some time[25]. On the large scale (larger than about 1µm), transport through conducting channels act "diffusive" because the mean free path of an electron is significantly smaller than the channel, and the electrons are scattered many times before leaving. The conductance of a channel is then determined by the familiar Ohm's law for materials. Smaller than this, channels act as "ballistic" conductors, where electrons travel through the whole channel without being scattered. To describe transport at this scale there exists a few transport theories. The Boltzmann transport equation (BTE) gives a semi-classical description of transport, and can be used for electrical transport[25], but currently is used mostly for describing phonons (vibrational motion)[26, 27], and the effects of coupling between electrons and phonons on electrical transport[28]. The state-of-the-art quantum description of electronic transport has for a long time been the Non Equilibrium Green's Function (NEGF) method[25, 29, 30] which describes a quantum system in contact with non-interacting leads. Green's function methods in general have been used a lot in quantum mechanics[31], mostly because it allows for easy incorporation of effects such as temperature[32], and contacts, which is what gives rise to the NEGF method. In the NEGF formalism however, the electronic structure in the channel, mostly the effects of electronic correlation, is not well described as the NEGF method is usually based on density functional theory. This has been somewhat addressed by applying a self-consistent GW self energy approach within the NEGF formalism[33–37], but there does not currently exist a framework for describing the electronic structure, and its properties, in systems undergoing transport. There is therefore still a lot of work to be done in this area, for example relating to the description of excited states and optical properties of the molecules in the channel.

1.2   Response Theory

In computational chemistry it is often desirable to be able to predict the effects of external potentials, such as external electric or magnetic fields, on a molecular system. Doing this, one can describe phenomena such as the electrical polarizability[38] and hyperpolarizabilities[39] of molecules due to an external electric field, or the magnetic polarizability[40], due to a magnetic field. Perhaps most notably it gives the framework to describe optical properties of molecules[41], since light (and other electromagnetic radiation) is just some oscillating electric and magnetic fields. Quantifying the responses molecular systems have to external potentials, with what is referred to as response functions, is what the field of response theory aims to achieve. Such external potentials are usually very small compared to the internal potentials in the molecule. Electric fields in the hydrogen atom are on the order of 10^{11}V m^{-1}[24] while the

electric field strengths in normal laser light is on the order of $1\,\mathrm{V\,m^{-1}}$. This is makes it possible to use perturbation theory to obtain expressions for the response functions.

Perturbation theory is an extremely powerful and widely used idea throughout quantum mechanics. It is used to include correlation energy in the electronic wavefunction of molecules in what is known as Møller-Plesset perturbation theory[42], and it is one of the fundamental pillars of quantum field theory[43]. The essence of perturbation theory is that there is some small perturbation to the system, and the problem of finding the change to the properties of the system is solved order by order. In the context of quantum chemistry the perturbation of the system is represented as a small perturbation to the system Hamiltonian so that

$$\hat{H} = \hat{H}^{(0)} + \hat{H}^{(1)} \tag{1.2.1}$$

where the unperturbed Hamiltonian of the system is the zeroth order Hamiltonian ($H^{(0)}$) and the perturbation is added as a first order Hamiltonian. In some cases one may chose to further divide the perturbation into even more orders. Using the expansion of the Hamiltonian, we expand the wave function and expectation values of observables into orders as well, such that

$$|\psi\rangle = |\psi\rangle^{(0)} + |\psi\rangle^{(1)} + |\psi\rangle^{(2)} + \dots, \qquad \langle A \rangle = \langle A \rangle^{(0)} + \langle A \rangle^{(1)} + \langle A \rangle^{(2)} \dots, \tag{1.2.2}$$

for some observable A. These expansions will go on to infinity, but in practice we will, truncate them to some order. The power of perturbation theory is that the equations for determining the correction at each order is found and solved separately.

1.2.1 Why Response Theory for Transport?

Transport of charge (electrical current) through a system, be that a large bulk system as a wire, or a nanoscale system as a molecule, is the response of the system to an external potential field, namely the voltage across the wire/molecule. This should therefore be possible to describe using response theory. Methods based on response theory have previously been used to describe current through molecular rectifiers[7]. In many cases, the DFT and GW NEGF methods are more then fine for predicting properties, however, they do not easily extend to include the description of optical properties. It is therefore desirable to develop a new method based on response theory, a framework where the description of optical is well understood, for describing transport processes. This will open up a new virtual playground for nanoelectronics/optoelectronics where we can investigate the properties of the molecules undergoing transport as we would any other system using response theory. This includes looking at how the optical properties of the molecules change as they undergo transport, and how the transport properties change in different electromagnetic fields. In this thesis, we illustrate the possibility of using the framework of response theory to describe molecular transport, comparing the theory and results with that of a simplified implementation of the NEGF method.

Chapter 2

Theoretical Background

In this chapter we introduce the necessary theory that lays the ground work that further chapters build upon. First we give a brief introduction to the main parts of electronic structure theory in the language of second quantization, including a description of post-Hartree-Fock correlated wave function models, discussing Configuration Interaction in particular. Further we go through the fundamentals of damped response theory, which introduces the equations that the main part of the thesis builds upon. Last we introduce the fundamentals of Green's function theory for quantum mechanics, which we build upon in later chapters where we discuss the NEGF method.

2.1   Electronic Structure Theory

The field of quantum chemistry is concerned with solving the molecular Schrödinger equation

$$\hat{H}|\psi(t)\rangle = i\hbar\frac{\partial}{\partial t}|\psi(t)\rangle, \tag{2.1.1}$$

for different systems. For molecules, the Hamiltonian operator, $\hat{H}$ (Total energy operator), contains the total energy of the electrons and nuclei of the molecule, which includes the kinetic energy of both $\hat{T}_e, \hat{T}_n$, and the potential energy between all the particles V_{ee}, V_{en}, V_{nn}. In electronic structure theory, we work within the Born-Oppenheimer approximation[44], which states that the wave function of the molecule can be separated into a product of the electronic part of the wave function and the nuclear part of the wavefunction

$$|\psi(r, R)\rangle = |\psi_e(r; R)\rangle \otimes |\psi_n(R)\rangle. \tag{2.1.2}$$

This way we can separate the problem of solving the molecular Schrödinger equation into first solving for the electronic wave function, then the nuclear wave function. In the field of electronic structure theory, we are concerned with the electronic wave function.

For most time independent molecular properties, such as ground state geometry, we do not need the full time dependent Schrödinger equation, but rather the time independent Schrödinger equation. We get this by assuming that the spatial electronic density, i.e. the modulus square

of the wave function, is constant, and that the only time dependence present is in the form of a phase factor $|\psi(t)\rangle = e^{-\frac{iEt}{\hbar}}|\psi\rangle$. Inserting this into the time dependent Schrödinger equation and cancelling the time dependent phase factor, we obtain the familiar time independent Schrödinger equation

$$\hat{H}|\psi\rangle = E|\psi\rangle. \tag{2.1.3}$$

In coordinate representation, this is a $3N$-dimensional partial differential equation so solving this analytically for many-electron systems is impossible, and directly solving exactly numerically is almost impossible. One of the most common approximations, which also serves as the starting point for many other methods, is the Hartree-Fock (HF) method[45]. In this method, the wave function is approximated by a single Slater-determinant and every electron effectively only feels the average potential of all the other electrons. This simplifies the problem from a single $3N$-dimensional problem to N 3-dimensional problems.

From the HF method we obtain a set of molecular orbitals (1-electron wave functions), which the Slater-determinant consists of. These are known as the occupied molecular orbitals. We also obtain a set of molecular orbitals which are not used in the Slater determinant, known as the virtual molecular orbitals. Using different combinations of occupied and virtual orbitals we can construct several Slater-determinants, or configuration state functions.

2.1.1 Second Quantization

As a way to neatly describe these different Slater-determinants we use the language of second quantization where in addition to the energy levels being quantized, the state itself is quantized using ladder operators. These ladder operators are the electron creation operator $a_{p\sigma}^{\dagger}$ which creates an electron in orbital number p with spin σ, and the annihilation operator $a_{p\sigma}$ which conversely removes an electron from the same spin orbital. A Slater-determinant is then represented by applying creation operators on the vacuum ket ($|\text{vac}\rangle$) which represents the Slater-determinants with 0 electrons. To represent the HF Slater-determinant we introduce the indexing convention where the indices i, j, k, l are used for occupied orbitals, a, b, c, d are used for the virtual orbitals and p, q, r, s are used as general indices. The HF state is then written as all the occupied creation operators applied on the vacuum ket

$$|\text{HF}\rangle = \left(\prod_i a_{i\alpha}^{\dagger} a_{i\beta}\right)|\text{vac}\rangle. \tag{2.1.4}$$

We can now also write the electronic Hamiltonian operator as

$$\hat{H} = h_{\text{nuc}} + \sum_{pq} h_{pq} E_{pq} + \frac{1}{2}\sum_{pqrs} g_{pqrs} e_{pqrs}. \tag{2.1.5}$$

h_{nuc} is the potential energy between the nuclei

$$h_{\mathrm{nuc}} = \frac{1}{2} \sum_{I \neq J} \frac{Z_I Z_J}{r_{IJ}}. \tag{2.1.6}$$

The one-electron integral matrix h_{pq} contains all of the integrals of the molecular orbitals over the one electron part of the normal Hamiltonian. This includes the kinetic energy of the electrons, and the potential energy between the electrons and the nuclei

$$h_{pq} = \langle \phi_p | \hat{h} | \phi_q \rangle. \tag{2.1.7}$$

The two-electron integral matrix g_{pqrs} contains the integrals over the two electron operator, which only contains the potential energy between all the electrons. We usually write this in Mulliken notation

$$g_{pqrs} = (pq|rs) = \langle \phi_p(1)\phi_r(2) | \hat{g} | \phi_q(1)\phi_s(2) \rangle. \tag{2.1.8}$$

The one- and two-electron singlet excitation operators (E_{pq} and e_{pqrs}) are defined as

$$E_{pq} = a_{p\alpha}^\dagger a_{q\alpha} + a_{p\beta}^\dagger a_{q\beta} = \sum_\sigma a_{p\sigma}^\dagger a_{q\sigma}, \tag{2.1.9}$$

$$e_{pqrs} = \sum_{\sigma\tau} a_{p\sigma}^\dagger a_{r\tau}^\dagger a_{s\tau} a_{q\sigma}. \tag{2.1.10}$$

Using these excitation operators, we can express the different N-electron Slater-determinants as different excitations of the HF determinant. Determinants differing by one spin orbital (singly excited) can be written as $|\phi_i^a\rangle = \frac{1}{\sqrt{2}} E_{ai} |\mathrm{HF}\rangle$, while those differing by two (doubly excited) as $|\phi_{ij}^{ab}\rangle = \frac{1}{2} E_{bj} E_{ai} |\mathrm{HF}\rangle$, etc. Most of the mathematics is done using some elementary commutator rules for the excitation, creation and annihilation operators. A defining property of the annihilation and creation operators is that they anti-commute, that is $a_{p\sigma}^\dagger a_{q\tau}^\dagger = -a_{q\tau}^\dagger a_{p\sigma}^\dagger$, giving the anti-symmetry of the wave function required by the Pauli principle for fermions. This is equivalent to the anti commutator being zero,

$$[a_{p\sigma}^\dagger, a_{q\tau}^\dagger]_+ = a_{p\sigma}^\dagger a_{q\tau}^\dagger + a_{q\tau}^\dagger a_{p\sigma}^\dagger = 0, \tag{2.1.11}$$

$$[a_{p\sigma}, a_{q\tau}]_+ = 0. \tag{2.1.12}$$

The other fundamental anti-commutator rule is:

$$[a_{p\sigma}, a_{q\tau}^\dagger]_+ = \delta_{pq}\delta_{\sigma\tau}, \tag{2.1.13}$$

where δ is the Kronecker delta. Using these commutators it is possible to derive some more useful commutator rules for the excitation operators

$$[E_{pq}, E_{rs}] = \delta_{qr} E_{ps} - \delta_{ps} E_{rq} \tag{2.1.14}$$

$$[E_{mn}, e_{pqrs}] = \delta_{pn} e_{mqrs} - \delta_{qm} e_{pnrs} + \delta_{rn} e_{pqms} - \delta_{sm} e_{pqrn} \tag{2.1.15}$$

7

2.1.2 Correlated Wave Function Models

As previously stated, the HF method is the starting point for so-called post-Hartree-Fock methods. These methods utilize that the set of possible Slater-determinants provides quite a good basis of anti-symmetric N-electron wave functions. In fact the set of all possible Slater-determinants is a complete basis of N-electron wave functions for a given basis of MOs. Taking into account all of the determinants is called the Full Configuration Interaction (FCI), but in practice this is computationally infeasible. The run time and memory requirements are binomial (far exceeding exponential), so even with recent advances in computing, this can only be used on small systems, with small basis sets, as a benchmark to test the accuracy of more computationally efficient methods. A simple solution to the problem is to include fewer determinants, where including only the ones differing from the HF determinant by a few spin orbitals leads to the truncated Configuration Interaction (CI) methods, such as CISD, where those determinants only differing from the HF state by 1 (singly excited) and 2 (doubly excited) spin orbitals. These methods have some problems, mainly not being size-consistent[46]. Other approaches include the aforementioned Møller-Plesset (MP) perturbation theory methods, as well as Coupled Cluster (CC) methods, which employ an exponential parameterization of the wave function, together with subspace projections, to obtain a corrected wave function. Both these methods have seen huge success, with MP2 being a very good method for describing properties of relatively large organic molecules[47, 48], and CC methods being a very good method of computing ground state properties of molecules[49] and more exotic properties, like light matter interaction in optical cavities[50].

In this thesis we use the Configuration Interaction truncated to Singles and Doubles (CISD) method for the ground state calculation for some systems. CI methods express the wavefunction as an explicit linear combination of Slater-determinants generated from a HF state, which we can write as

$$|\psi\rangle = C_{\mathrm{HF}}|\mathrm{HF}\rangle + \sum_{ai} C_i^a |\phi_i^a\rangle + \sum_{abij} C_{ij}^{ab} |\phi_{ij}^{ab}\rangle + \dots \quad (2.1.16)$$

The variational theorem now states that the expectation value of the energy is always greater than, or equal to, the energy of the exact ground state, that is

$$\langle\psi|\hat{H}|\psi\rangle \geq E_0, \quad (2.1.17)$$

so to get as close as possible to the actual ground state, we the minimize this expectation value variationally with respect to the expansion coefficients, while keeping the wave function normalized. Truncated CI methods are obtained by simply truncating the linear combination in eq. (2.1.16) to only include certain Slater-determinants. In CISD we only include single and double excited determinants, so the expansion of the wave function is

$$|\psi\rangle = C_{\mathrm{HF}}|\mathrm{HF}\rangle + \sum_{ai} C_i^a |\phi_i^a\rangle + \sum_{abij} C_{ij}^{ab} |\phi_{ij}^{ab}\rangle. \quad (2.1.18)$$

2.2 Response Theory

A time dependent quantum system is described by the electronic Schrödinger equation

$$\hat{H}|\psi(t)\rangle = i\hbar \frac{\partial}{\partial t}|\psi(t)\rangle, \tag{2.2.1}$$

where $\hat{H}$ is the system Hamiltonian. Depending on the system, the Hamiltonian may or may not be time dependent. We can separate the Hamiltonian into a time independent ground state Hamiltonian ($\hat{H}^{(0)}$) and a (possibly) time dependent perturbation ($\hat{H}^{(1)}$) such that

$$\hat{H} = \hat{H}^{(0)} + \hat{H}^{(1)}(t). \tag{2.2.2}$$

We here assume that we posses the solutions of the zeroth order time independent Schrödinger equation, i.e. we have the eigenfunctions and eigenvalues of $\hat{H}^{(0)}$,

$$\hat{H}^{(0)}|n\rangle = E_n|n\rangle, \tag{2.2.3}$$

and in particular the zeroth order ground state $|0\rangle$. This might for example be a HF, CI, CC or Multi Configurational (MCSCF) state. A common parametrization of the wave function ($|\psi(t)\rangle$) is by directly expressing it as a linear combination of the zeroth order eigenfunctions as

$$|\psi(t)\rangle = \sum_n c_n(t)|n\rangle, \tag{2.2.4}$$

where the time dependence is captured in the coefficients $c_n(t)$. The coefficients can be found by projecting the wave function onto each of the eigenfunctions,

$$\langle m|\psi\rangle = \sum_n c_n \langle m|n\rangle = c_m, \tag{2.2.5}$$

which is easily seen by the orthogonality of the eigenfunctions. This approach is very common when explicitly describing the time evolution of systems where the Hamiltonian is time independent and we can assume the system having a known initial condition $|\psi(0)\rangle$. This way we can determine the initial expansion coefficients from eq. (2.2.5), and because of the time independent Hamiltonian, the time evolution of the coefficients is simply the time evolution phase factor for the corresponding eigenfunction $e^{-\frac{iEt}{\hbar}}$. However, to keep the wave function normalized, the following constraint on the coefficients has to be fulfilled,

$$\sum_n |c_n|^2 = 1. \tag{2.2.6}$$

This makes this parametrization somewhat inconvenient to use for the perturbation theory we will employ in this thesis. A more convenient approach that we will use, is to parameterize the wave function by a unitary transformation of the ground state $|0\rangle$,

$$|\psi(t)\rangle = e^{i\hat{P}(t)}|0\rangle, \tag{2.2.7}$$

9

where $\hat{P}(t)$ is a hermitian operator that captures the time dependence. In this parametrization we avoid the need for a separate normalization constraint which we can see by,

$$\langle\psi|\psi\rangle = \langle 0|e^{-i\hat{P}(t)}e^{i\hat{P}(t)}|0\rangle = \langle 0|0\rangle = 1. \tag{2.2.8}$$

One way to parameterize $\hat{P}(t)$ is[51]

$$\hat{P}(t) = \sum_{n>0}\left(P_n(t)|n\rangle\langle 0| + P_n^*(t)|0\rangle\langle n|\right). \tag{2.2.9}$$

We can reformulate this parametrization in terms of second quantization as[39]

$$\hat{P}(t) = \sum_{ai}\left(\kappa_{ai}E_{ai} + \kappa_{ia}E_{ia}\right) + \sum_{aibj}\left(S_{aibj}E_{ai}E_{bj} + S_{jbia}E_{jb}E_{ia}\right) + \dots \tag{2.2.10}$$

Where the coefficients $(\kappa, S, \dots)$ are functions of time, and constrained to make $\hat{P}(t)$ hermitian $(\kappa_{ai} = \kappa_{ia}^*, S_{aibj} = S_{jbia}^*)$. Similar to CI we can truncate the amount of operators to include in the expansion of $\hat{P}$, usually for the sake of being easier to implement and more computationally efficient at the cost of accuracy. We discuss the truncation of this in the following chapter.

To be able to determine the coefficients in a peturbative manner, we must expand them in different orders. We then have,

$$\kappa_{ai} = \kappa_{ai}^{(0)} + \kappa_{ai}^{(1)} + \kappa_{ai}^{(2)} + \dots, \tag{2.2.11a}$$
$$S_{aibj} = S_{aibj}^{(0)} + S_{aibj}^{(1)} + S_{aibj}^{(2)} + \dots, \tag{2.2.11b}$$

which gives

$$\hat{P}(t) = \hat{P}^{(0)}(t) + \hat{P}^{(1)}(t) + \hat{P}^{(2)}(t) + \dots, \tag{2.2.12}$$

with

$$\hat{P}^{(n)}(t) = \sum_{ai}\left(\kappa_{ai}^{(n)}E_{ai} + \kappa_{ia}^{(n)}E_{ia}\right) + \sum_{aibj}\left(S_{aibj}^{(n)}E_{ai}E_{bj} + S_{jbia}^{(n)}E_{jb}E_{ia}\right) + \dots \tag{2.2.13}$$

By assuming $|0\rangle$ to solve the zeroth order equation, all zeroth order terms will disappear[39]. To illustrate this we expand the operator

$$e^{i\hat{P}} = 1 + i\hat{P} - \frac{\hat{P}^2}{2} + \dots, \tag{2.2.14}$$

and using eq. (2.2.12), we can expand $\hat{P}^n$ into a zeroth order term and a term containing all higher orders

$$\hat{P}^n = \left(\hat{P}^{(0)}(t) + \hat{P}^{(1)}(t) + \hat{P}^{(2)}(t) + \dots\right)^n = \hat{P}^{(0)n} + \hat{\Omega}^{(1)}. \tag{2.2.15}$$

This way we can also separate the exponential expansion into a zeroth order term and a higher order term,

$$e^{i\hat{P}} = e^{i\hat{P}^{(0)}} + \hat{\Omega}^{(1)}. \tag{2.2.16}$$

Inserting this into the Schrödinger equation (eq. (2.2.1)), we can separate the zeroth order equation as,

$$\hat{H}^{(0)} e^{iP^{(0)}(t)}|0\rangle = i\hbar \frac{\partial}{\partial t} e^{iP^{(0)}(t)}|0\rangle, \tag{2.2.17}$$

but $|0\rangle$ already fulfils the zeroth order equation by itself, meaning the equation

$$\hat{H}^{(0)} e^{-i\frac{Et}{\hbar}}|0\rangle = i\hbar \frac{\partial}{\partial t} e^{-i\frac{Et}{\hbar}}|0\rangle, \tag{2.2.18}$$

is fulfilled. This means that the zeroth order part of $\hat{P}(t)$ only includes the total phase factor of the wave function, which has no impact on the observables we are considering in this thesis. It is, however, important to note that the assumption that the ground state, $|0\rangle$, is a solution to the zeroth order function breaks down when the ground state is approximated by for example CISD. For quantitatively accurate results, this deviation will need to be considered and zeroth order orbital rotations and configurations might need to be included, but we are presenting proof of concept calculations where simplicity for the sake of understandability and ease of implementation takes precedence over accuracy. Thus we will be neglecting the zeroth order terms of $\hat{P}(t)$ so that we are left with

$$\hat{P}(t) = \hat{P}^{(1)}(t) + \hat{P}^{(2)}(t) + \dots \tag{2.2.19}$$

2.2.1 Ehrenfest Theorem and First Order Equation

Response theory is concerned with finding response functions for observables, $\delta\langle\hat{A}\rangle$, which gives the change in the expectation value of an observable, A, as a response to a perturbation. The usual starting point for this is looking at the time derivative of the expectation value, $\frac{\partial}{\partial t}\langle\hat{A}\rangle$. This leads to the generalized Ehrenfest theorem, being the key equation that we use to determine the response functions. The generalized Ehrenfest theorem states

$$\frac{\partial}{\partial t}\langle\hat{A}\rangle = \frac{1}{i\hbar}\langle[\hat{A}, \hat{H}]\rangle, \tag{2.2.20}$$

for a time independent operator, $\hat{A}$. In many cases, a dampening factor, γ, is added to the equation to account for the finite lifetimes of energy levels that we observe in real systems[52]. This factor is added phenomenologically to account for all the interactions the system has with the environment, such as collisions between molecules, that would lead to the energy levels having finite lifetimes. This dampening parameter is often necessary to include to avoid singularities, which we will see below. In the context of electronic transport, the interactions that would lead to the finite lifetimes is the interaction with electron reservoirs creating an

open system. For steady state transport it would not make sense to have transport if electrons could not jump between energy levels in a finite amount of time. Including this dampening factor, we obtain what we may refer to as the damped Ehrenfest theorem that looks like

$$\frac{\partial}{\partial t}\langle \hat{A} \rangle = \frac{1}{i\hbar}\langle [\hat{A}, \hat{H}] \rangle + \gamma \langle \hat{A} \rangle. \tag{2.2.21}$$

These equations are what we use to determine expressions for the parametrization coefficients (eq. (2.2.7)). Here we present the derivation for the first order equations. To obtain the equation for determining the expansion coefficients to first order, we insert the wave function parameterization into the damped Ehrenfest theorem (eq. (2.2.21)). We then have two expectation values to expand. We start by inserting the parametrization into $\langle \hat{A} \rangle$,

$$\langle A \rangle = \langle \psi | \hat{A} | \psi \rangle = \langle 0 | e^{-i\hat{P}} \hat{A} e^{i\hat{P}} | 0 \rangle, \tag{2.2.22}$$

then using the Baker-Campbell-Hausdorf expansion,

$$e^{-i\hat{P}} \hat{A} e^{i\hat{P}} = \hat{A} + i[\hat{A}, \hat{P}] - \frac{1}{2}[[\hat{A}, \hat{P}], \hat{P}] - \frac{i}{3!}[[[\hat{A}, \hat{P}], \hat{P}], \hat{P}] + \dots, \tag{2.2.23}$$

we get

$$\langle \hat{A} \rangle = \langle 0 | \hat{A} | 0 \rangle + i \langle 0 | [\hat{A}, \hat{P}] | 0 \rangle + \dots \tag{2.2.24}$$

Separating $\hat{P}$ into orders and grouping the expression by order, we get the zeroth and first order expansion

$$\langle \hat{A} \rangle^{(0)} = \langle 0 | \hat{A} | 0 \rangle, \tag{2.2.25a}$$

$$\langle \hat{A} \rangle^{(1)} = i \langle 0 | [\hat{A}, \hat{P}^{(1)}] | 0 \rangle. \tag{2.2.25b}$$

Next we expand $\langle [\hat{A}, \hat{H}] \rangle$ similarly to get

$$\langle [\hat{A}, \hat{H}] \rangle^{(0)} = \langle 0 | [\hat{A}, \hat{H}^{(0)}] | 0 \rangle \tag{2.2.26a}$$

$$\langle [\hat{A}, \hat{H}] \rangle^{(1)} = \langle 0 | [\hat{A}, \hat{H}^{(1)}] | 0 \rangle + i \langle 0 | [[\hat{A}, \hat{H}^{(0)}], \hat{P}^{(1)}] | 0 \rangle \tag{2.2.26b}$$

Now we have what we need to write down the first order equation

$$\frac{\partial}{\partial t}\langle \hat{A} \rangle^{(1)} = \frac{1}{i\hbar}\langle [\hat{A}, \hat{H}] \rangle^{(1)} + \gamma \langle \hat{A} \rangle^{(1)}. \tag{2.2.27}$$

Inserting the first order expansions we get

$$i\frac{\partial}{\partial t}\langle 0 | [\hat{A}, \hat{P}^{(1)}] | 0 \rangle = \frac{1}{i\hbar}\langle 0 | [\hat{A}, \hat{H}^{(1)}] | 0 \rangle + \frac{1}{\hbar}\langle 0 | [[\hat{A}, \hat{H}^{(0)}], \hat{P}^{(1)}] | 0 \rangle + i\gamma \langle 0 | [\hat{A}, \hat{P}^{(1)}] | 0 \rangle. \tag{2.2.28}$$

For a given operator, $\hat{A}$, this gives a single equation. To get enough equations, we insert all of the excitation and de-excitation operators from the parametrization $\hat{P}(t)$ $(E_{ai}, E_{ia}, E_{ai}E_{bj}, \dots)$. This will give the right amount of equations for a square linear system of differential equations for the coefficients. To express this nicely in a matrix equation we introduce the vectors

$$\boldsymbol{\alpha}^{(n)}(t) = \begin{pmatrix} \kappa_{ai}^{(n)} \\ \vdots \\ S_{aibj}^{(n)} \\ \vdots \\ \kappa_{ia}^{(n)} \\ \vdots \\ S_{jbia}^{(n)} \\ \vdots \end{pmatrix}, \qquad \boldsymbol{\Lambda} = \begin{pmatrix} E_{ai} \\ \vdots \\ E_{ai}E_{bj} \\ \vdots \\ E_{ia} \\ \vdots \\ E_{jb}E_{ia} \\ \vdots \end{pmatrix}, \tag{2.2.29}$$

with $\boldsymbol{\alpha}$ being the column vector of coefficients, and $\boldsymbol{\Lambda}$ being the row vector of excitation/de-excitation operators. This way we can replace $\hat{A}$ with $\Lambda_\mu^\dagger$ and express $\hat{P}^{(n)}(t)$ as

$$\hat{P}^{(n)}(t) = \sum_\nu \alpha_\nu^{(n)} \Lambda_\nu. \tag{2.2.30}$$

Inserting this into the first order eq. (2.2.28) we get

$$i \sum_\nu \langle 0|[\Lambda_\mu^\dagger, \Lambda_\nu]|0\rangle \frac{\partial \alpha_\nu^{(1)}}{\partial t} =$$
$$\frac{1}{i\hbar} \langle 0|[\Lambda_\mu^\dagger, \hat{H}^{(1)}]|0\rangle + \frac{1}{\hbar} \sum_\nu \langle 0|[[\Lambda_\mu^\dagger, \hat{H}^{(0)}], \Lambda_\nu]|0\rangle \alpha_\nu^{(1)} + i\gamma \sum_\nu \langle 0|[\Lambda_\mu^\dagger, \Lambda_\nu]|0\rangle \alpha_\nu^{(1)}. \tag{2.2.31}$$

We now define the matrices $\boldsymbol{S}$ and $\boldsymbol{M}$ as well as the vector $\boldsymbol{V}$ as

$$S_{\mu\nu} = \langle 0|[\Lambda_\mu^\dagger, \Lambda_\nu]|0\rangle, \qquad M_{\mu\nu} = \langle 0|[[\Lambda_\mu^\dagger, \hat{H}^{(0)}], \Lambda_\nu]|0\rangle, \qquad V_\mu = \langle 0|[\Lambda_\mu^\dagger, \hat{H}^{(1)}]|0\rangle. \tag{2.2.32}$$

We can now cast eq. (2.2.31) in matrix form as

$$i\boldsymbol{S}\frac{\partial \boldsymbol{\alpha}}{\partial t} = \frac{1}{i\hbar}\boldsymbol{V} + \frac{1}{\hbar}\boldsymbol{M}\boldsymbol{\alpha} + i\gamma\boldsymbol{S}\boldsymbol{\alpha}. \tag{2.2.33}$$

We are not interested in the explicit time evolution of the wave function, but rather the response after some infinite time. For this it is more convenient to have the equation in the frequency domain rather than the time domain. Time dependent perturbations representing some frequencies of light, for example, is much more conveniently represented as functions of frequency rather than time. This is done by applying the Fourier transform to the equation

$$-\omega\boldsymbol{S}\boldsymbol{\alpha} = \frac{1}{i\hbar}\boldsymbol{V} + \frac{1}{\hbar}\boldsymbol{M}\boldsymbol{\alpha} + i\gamma\boldsymbol{S}\boldsymbol{\alpha} \tag{2.2.34}$$

which is rearranged into

$$(\boldsymbol{M} + \hbar(\omega + i\gamma)\boldsymbol{S})\boldsymbol{\alpha} = i\boldsymbol{V}. \tag{2.2.35}$$

This is similar to equation 44 in[39], but with γ serving as an imaginary part to the frequency. It is now important to keep in mind that both $\boldsymbol{\alpha}$ and $\boldsymbol{V}$ are now functions of the frequency ω. The process of solving the equation given a perturbation, $\boldsymbol{V}(t)$, would be to find its Fourier transform, $\boldsymbol{V}(\omega)$, solve for $\boldsymbol{\alpha}(\omega)$, then take the inverse Fourier transform to get $\boldsymbol{\alpha}(t)$.

The necessity of the dampening parameter, γ, is now also more apparent as this equation is only solvable when the matrix $(\boldsymbol{M} + \hbar(\omega + i\gamma))$ is non-singular. If $\gamma = 0$, the matrix is singular if $\hbar\omega$ is a generalized eigenvalue of M, so by adding a non-zero dampening, we avoid going directly through the eigenvalues, making it possible to integrate over all frequencies. If we have the special case where $\boldsymbol{V}(t) = \boldsymbol{V}$ is a constant (time independent) perturbation, we have

$$\boldsymbol{V}(\omega) = \sqrt{2\pi}\delta(\omega)\boldsymbol{V}, \tag{2.2.36}$$

where $\delta(\omega)$ is the Dirac-delta function. The equation can then be solved as

$$\boldsymbol{\alpha}(\omega) = i\sqrt{2\pi}\delta(\omega)(\boldsymbol{M} + i\hbar\gamma\boldsymbol{S})^{-1}\boldsymbol{V}, \tag{2.2.37}$$

where we can apply the inverse Fourier transform to obtain a time independent $\boldsymbol{\alpha}$

$$\boldsymbol{\alpha}(t) = i(\boldsymbol{M} + i\hbar\gamma\boldsymbol{S})^{-1}\boldsymbol{V}. \tag{2.2.38}$$

We can also recognize this as a steady state solution of eq. (2.2.33). The solutions of this equation gives us the first order correction to the wave function which we use to further calculate the first order corrections to properties like for example the energy of the system. In this thesis we use the coefficients to determine the amount of electrons transported between parts of the system.

2.3 Green's Function Theory

Green's function methods are common throughout many fields in physics, electrical engineering, and quantum mechanics, as they are in general a useful way to approach problems where linear differential equations show up. Here we present the relevant background for the Non-Equilibrium Green's Function method that we use later in this thesis.

A Green's function is defined as being the solution to a linear differential equation of the form

$$(E - \hat{H}(r))G(r, r'; E) = \delta(r - r'), \tag{2.3.1}$$

where H is a linear operator, G is the Green's function, E is some parameter (real or complex) and δ is the Dirac delta function[31]. For operators in matrix form we define the Green's function matrix as the solution of the equation[53]

$$(E\boldsymbol{I} - \boldsymbol{H})\boldsymbol{G}(E) = \boldsymbol{I}, \tag{2.3.2}$$

where $\boldsymbol{H}$ and $\boldsymbol{G}$ are replaced with their matrices, and the Dirac delta function is replaced with the identity matrix. That is, the Green's function matrix is the inverse of the matrix $(E\boldsymbol{I} - \boldsymbol{H})$,

$$\boldsymbol{G}(E) = (E\boldsymbol{I} - \boldsymbol{H})^{-1}. \tag{2.3.3}$$

When we in this thesis refer to the Green's function, we refer to this matrix. This Green's function gives us the solutions to the Schrödinger equation with a constant perturbation $\boldsymbol{s}$[25]

$$\boldsymbol{H}\boldsymbol{\psi} = E\boldsymbol{\psi} + \boldsymbol{s} \tag{2.3.4}$$

as we can rewrite this into

$$(E\boldsymbol{I} - \boldsymbol{H})\boldsymbol{\psi} = -\boldsymbol{s} \quad \Rightarrow \quad \boldsymbol{\psi} = -\boldsymbol{G}(E)\boldsymbol{s}. \tag{2.3.5}$$

An important quantity we can obtain from the Green's function is what is known as the **spectral function**, which is the anti-hermitian part of the Green's function[25]

$$\boldsymbol{A} = i(\boldsymbol{G} - \boldsymbol{G}^{\dagger}). \tag{2.3.6}$$

For this to make sense, the Green's function needs to be non-hermitian, but the inverse of a hermitian matrix is hermitian, so $(E\boldsymbol{I} - \boldsymbol{H})$ must be non-hermitian. This is done by adding a small imaginary part to the energy parameter $(E \rightarrow E + i\eta)$. This η is usually made to approach zero. The resulting limits gives rise to the solutions of the normal Schrödinger equation $H\psi = E\psi$. This can be seen in section 2.3 of [53]. For many non-equilibrium situations, however, this parameter is not set to approach zero, but rather exist as a finite dampening parameter, leading to energy levels having finite lifetimes and being broadened, similar to what we have seen for damped response theory above (eq. (2.2.21)).

Chapter 3

Transport from Response Theory

In this chapter we use the equations presented in section 2.2 to obtain an expression for the electronic transport between two subsystems of a closed system. This consists of a few main parts. First we will briefly discuss the truncated version of the wave function parametrization from eq. (2.2.7) that we have used here. We also give a derivation of the damped Ehrenfest theorem we presented in eq. (2.2.21) to highlight some of the main similarities to the NEGF method. Then we need to explicitly find the coefficients of our truncated parametrization of the perturbed wavefunction. This involves finding explicit expressions for the matrix elements of the three matrices in eq. (2.2.32), which are used in eq. (2.2.38) to solve for the parametrization coefficients contained in $\boldsymbol{\alpha}$. We then finally need an expression for the transport based on this parametrization of the perturbed wave function, which needs an explicit description of how we partition the system into subsystems that the electrons will be transported between.

3.1   Truncation of the Parametrization

As discussed in the previous chapter, we may truncate the expansion of the hermitian operator, $\hat{P}(t)$, in the parametrization for the perturbed wave function. In this thesis we are interested in presenting the simplest possible proof-of-concept method that yield any interesting results. We will therefore be using an aggressively truncated parametrization, only including orbital rotations in the expansion of $\hat{P}(t)$ such that it now looks like

$$\hat{P}(t) = \sum_{ai} (\kappa_{ai} E_{ai} + \kappa_{ia} E_{ia}). \tag{3.1.1}$$

This further leads to the $\boldsymbol{\alpha}(t)$ and $\boldsymbol{\Lambda}$ vectors being simplified to

$$\boldsymbol{\alpha}^{(n)}(t) = \begin{pmatrix} \kappa_{ai}^{(n)} \\ \vdots \\ \kappa_{ia}^{(n)} \\ \vdots \end{pmatrix}, \qquad \boldsymbol{\Lambda} = \begin{pmatrix} E_{ai} \\ \vdots \\ E_{ia} \\ \vdots \end{pmatrix}, \tag{3.1.2}$$

which will lead to the expressions for the matrix elements in eq. (2.2.32) being significantly easier to compute, which we will see below.

3.2 Derivation of the Damped Ehrenfest Theorem

In this section we give a simple derivation of the Ehrenfest theorem with the purpose of highlighting some key similarities between the damped Ehrenfest theorem, and the equation we use in the NEGF method to get an expression for the steady state current through a channel. We begin by applying the product rule on the time derivative of the expectation value of some general time independent operator $\hat{A}$

$$\frac{\partial}{\partial t}\langle\hat{A}\rangle = \frac{\partial}{\partial t}\langle\psi|\hat{A}|\psi\rangle = \left(\frac{\partial}{\partial t}\langle\psi|\right)\hat{A}|\psi\rangle + \langle\psi|\left(\hat{A}\frac{\partial}{\partial t}|\psi\rangle\right). \tag{3.2.1}$$

We can then use the time dependent Schrödinger equation, and its adjoint

$$\frac{\partial}{\partial t}|\psi\rangle = \frac{1}{i\hbar}\hat{H}|\psi\rangle \quad\Rightarrow\quad \frac{\partial}{\partial t}\langle\psi| = \left(\frac{\partial}{\partial t}|\psi\rangle\right)^{\dagger} = \left(\frac{1}{i\hbar}\hat{H}|\psi\rangle\right)^{\dagger} = -\frac{1}{i\hbar}\langle\psi|\hat{H}^{\dagger} \tag{3.2.2}$$

to replace the time derivatives, giving us

$$\frac{\partial}{\partial t}\langle\hat{A}\rangle = -\frac{1}{i\hbar}\langle\psi|\hat{H}^{\dagger}\hat{A}|\psi\rangle + \frac{1}{i\hbar}\langle\psi|\hat{A}\hat{H}|\psi\rangle = \frac{1}{i\hbar}\langle\psi|\hat{A}\hat{H} - \hat{H}^{\dagger}\hat{A}|\psi\rangle \tag{3.2.3}$$

which for a hermitian Hamiltonian becomes the familiar Ehrenfest theorem in eq. (2.2.20). However if the Hamiltonian contains a non-hermitian part, $\hat{\Sigma}$, such that we can replace the Hamiltonian as

$$\hat{H} \rightarrow \hat{H} + \hat{\Sigma}, \tag{3.2.4}$$

eq. (3.2.3) would simplify to

$$\frac{\partial}{\partial t}\langle\hat{A}\rangle = \frac{1}{i\hbar}\langle[\hat{A},\hat{H}]\rangle + \frac{1}{i\hbar}\langle\hat{A}\hat{\Sigma} - \hat{\Sigma}^{\dagger}\hat{A}\rangle. \tag{3.2.5}$$

The reason for wanting to consider a non-hermitian Hamiltonian, is again to draw parallels to the NEGF method, where the addition of a non-hermitian term to the Hamiltonian is how the incorporation of contacts to electron reservoirs is done. If the non-hermitian part were to take a particularly simple form, for example an imaginary number $\hat{\Sigma} = i\hbar\frac{\gamma}{2}$, eq. (3.2.5) would further simplify to

$$\frac{\partial}{\partial t}\langle\hat{A}\rangle = \frac{1}{i\hbar}\langle[\hat{A},\hat{H}]\rangle + \gamma\langle\hat{A}\rangle, \tag{3.2.6}$$

which is the damped Ehrenfest theorem from eq. (2.2.21). Now, if we go back to eq. (3.2.5) and exchange the general operator for a state change operator $\hat{A} = |n\rangle\langle m|$, we can rearrange eq. (3.2.5) into

$$\frac{\partial}{\partial t}\langle m|\hat{D}|n\rangle = \frac{1}{i\hbar}\langle m|[\hat{H},\hat{D}]|n\rangle + \frac{1}{i\hbar}\langle m|\hat{\Sigma}\hat{D} - \hat{D}\hat{\Sigma}^{\dagger}|n\rangle, \tag{3.2.7}$$

where $\hat{D}$ is the density operator $|\psi\rangle\langle\psi|$. This is element (m, n) of the same equation with the operators in matrix form

$$\frac{\partial}{\partial t}\boldsymbol{D} = \frac{1}{i\hbar}[\boldsymbol{H}, \boldsymbol{D}] + \frac{1}{i\hbar}\left(\boldsymbol{\Sigma}\boldsymbol{D} - \boldsymbol{D}\boldsymbol{\Sigma}^\dagger\right), \tag{3.2.8}$$

which describes the time evolution of the density matrix. We will see in the next chapter how this equation is very similar to the equation used in the NEGF formalism to describe the time evolution of the density matrix.

3.3   Expressions for Matrix Elements

Detailed derivations of the matrix elements of $\boldsymbol{S}$, $\boldsymbol{M}$ and $\boldsymbol{V}$ can be found in appendix A. Here we present the main points of the derivation as well as the resulting expressions. The expressions for the matrix elements that we present here are heavily dependent on our specific choice of parametrization of the perturbed wave function, but depends on the MO-integrals and one- and two-electron density matrices of a general post-HF ground state wave function. All the matrices are written as 2 by 2 block matrices. This is a result of the $\boldsymbol{\Lambda}$ vector containing two major blocks, which we refer to as the exctiation and de-excitation operators written as

$$\boldsymbol{\Lambda} = \begin{pmatrix} \boldsymbol{\Lambda}^{(e)} \\ \boldsymbol{\Lambda}^{(d)} \end{pmatrix}, \tag{3.3.1}$$

where $\boldsymbol{\Lambda}^{(e)}$ is the excitation block of $\boldsymbol{\Lambda}$ as it contains all the excitation operators E_{ai}, and likewise the de-excitation block $\boldsymbol{\Lambda}^{(d)}$ contains all the de-excitation operators E_{ia}. The blocks of the matrices are then defined by if which elements of $\boldsymbol{\Lambda}$ are used. For the (de) block of a matrix, the first element comes from the $\boldsymbol{\Lambda}^{(d)}$ and the second is from $\boldsymbol{\Lambda}^{(e)}$. The three block matrices then generally looks like

$$\boldsymbol{S} = \begin{pmatrix} \boldsymbol{S}^{(ee)} & \boldsymbol{S}^{(ed)} \\ \boldsymbol{S}^{(de)} & \boldsymbol{S}^{(dd)} \end{pmatrix}, \qquad \boldsymbol{M} = \begin{pmatrix} \boldsymbol{M}^{(ee)} & \boldsymbol{M}^{(ed)} \\ \boldsymbol{M}^{(de)} & \boldsymbol{M}^{(dd)} \end{pmatrix}, \qquad \boldsymbol{V} = \begin{pmatrix} \boldsymbol{V}^{(e)} \\ \boldsymbol{V}^{(d)} \end{pmatrix}. \tag{3.3.2}$$

The expressions for elements of the matrices are thus given block by block.
The $\boldsymbol{S}$ matrix is given by

$$\boldsymbol{S} = \begin{pmatrix} \boldsymbol{S}^{(ee)} & \boldsymbol{0} \\ \boldsymbol{0} & -\boldsymbol{S}^{(ee)}, \end{pmatrix}, \qquad S^{(ee)}_{\mu\nu} = \delta_{ij}D^{(0)}_{ab} - \delta_{ab}D^{(0)}_{ji}. \tag{3.3.3}$$

The M matrix is given by

$$\boldsymbol{M} = \begin{pmatrix} \boldsymbol{M}^{(ee)} & \boldsymbol{M}^{(de)\dagger} \\ \boldsymbol{M}^{(de)} & \boldsymbol{M}^{(ee)\dagger}, \end{pmatrix} \tag{3.3.4a}$$

$$M_{\mu\nu}^{(ee)} = h_{ab}D_{ij}^{(0)} + h_{ji}D_{ba}^{(0)}$$
$$+ \sum_{pq}\left(g_{pqab}d_{pqij}^{(0)} + g_{pbaq}d_{pjiq}^{(0)} - g_{jpaq}d_{bpiq}^{(0)} + g_{pqji}d_{pqba}^{(0)} - g_{pbqi}d_{pjqa}^{(0)} + g_{jpqi}d_{bpqa}^{(0)}\right)$$
$$-\delta_{ij}\sum_{p}h_{ap}D_{bp}^{(0)} - \delta_{ab}\sum_{p}h_{pi}D_{pj}^{(0)} - \delta_{ij}\sum_{pqr}g_{pqar}d_{pqbr}^{(0)} - \delta_{ab}\sum_{pqr}g_{pqri}d_{pqrj}^{(0)}. \tag{3.3.4b}$$

$$M_{\mu\nu}^{(de)} = h_{ib}D_{aj}^{(0)} + h_{ja}D_{bi}^{(0)}$$
$$+ \sum_{pq}\left(g_{pqib}d_{pqaj}^{(0)} + g_{pbiq}d_{pjaq}^{(0)} - g_{jpiq}d_{bpaq}^{(0)} + g_{pqja}d_{pqbi}^{(0)} - g_{pbqa}d_{pjqi}^{(0)} + g_{jpqa}d_{bpqi}^{(0)}\right) \tag{3.3.4c}$$

The elements of the vector $\boldsymbol{V}$ depends on the specific form of the perturbation operator, $\hat{H}^{(1)}$. Here we have assumed it taking the form of an effective one-electron operator of the form

$$\hat{H}^{(1)} = \sum_{pq} W_{pq}E_{pq}, \tag{3.3.5}$$

where we have considered two special cases of this W_{pq} matrix, which we discuss in detail below. For a general matrix $\boldsymbol{W}$ the expression for the vector $\boldsymbol{V}$ is given by

$$\boldsymbol{V} = \begin{pmatrix} \boldsymbol{V}^{(e)} \\ -\boldsymbol{V}^{(e)*} \end{pmatrix} \qquad V_\mu^{(e)} = V_{ai}^{(e)} = \sum_p W_{ap}D_{ip}^{(0)} - W_{pi}D_{pa}^{(0)} \tag{3.3.6}$$

where $\boldsymbol{D}^{(0)}$ is the the one electron density matrix of the ground state wave function.

3.4 Partitioning of the System

Since we are interested in looking at the transport of electrons caused by the perturbation, we need a partitioning of the system into subsystems that electrons can move between. In this thesis we will be considering a partitioning into two subsystems, where we are looking for the transport of electrons from one of the subsystems to the other as illustrated in fig. 3.4.1. This type of system is relevant for describing transport processes like redox reactions. For processes involving steady state current it would be more natural to divide the system into three subsystems, like we do for the NEGF method which is discussed below. That way we could have a system where electrons on average move from system 1 to system 2, and further from system 2 to system 3 as illustrated in fig. 4.1.1. For other systems, perhaps something like a molecular transistor, it might make sense to divide into even more subsystems.

All of the occupied and virtual orbitals of the system is partitioned such that each orbital is assigned to a single subsystem. This is a simple and convenient partitioning which is sufficient when looking at weakly coupled molecules. When systems are highly coupled, for example when there are covalent bonds between the two systems, the picture is more complex, but this will be a reasonable assumption when the orbitals are localized to one of the subsystems. This can be

improved upon by running some orbital localization scheme[54], but this will not be discussed here. Orbitals are assigned to the subsystem it has the most atomic orbital contributions from. For the mathematical notation we will be considering one of the two subsystems as the "main" system, which the equations are with respect to. This main system is often referred to as the device, with the remaining subsystem referred to as the contact or environment subsystem, depending on the context. We label the orbital indices corresponding to the main system with a bar $(\bar{p}, \bar{a}, \bar{i})$ and orbital indices of the other system with tildes $(\tilde{p}, \tilde{a}, \tilde{i})$, which can be seen in fig. 3.4.1. For indices running over the total system, normal indices will be used (p, a, i).
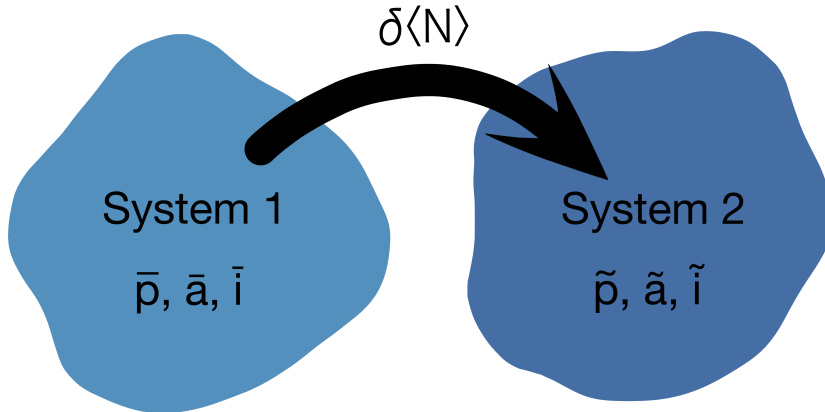

Figure 3.4.1: System partitioned into two subsystems. The arrow depicts electronic density moving from system 1 to system 2 with the response of the average number of electrons in system 1 being reduced by $\delta\langle N\rangle$ and similarly increased by the same amount in system 2. Credit: Ylva Os

3.4.1 Special cases of perturbation operators

For any practical application, the exact form of the perturbation operator would be derived from some physical interaction, possibly to do with the dipole operator, but for the proof-of-concept work here, we assume some simple special cases of the matrix $\boldsymbol{W}$. The first special case is the $\boldsymbol{W}$ matrix being diagonal where some orbitals are raised by some potential shift, and the other orbitals lowered by the same amount. This is a simplified model for having an external voltage applied to the system, which should raise the potential energy of one part of the system, and lower the potential energy of another part of the system. For a real system connected to some contacts applying the voltage, the increases and decreases would of course not be uniform as we are doing here, but rather having parts of the system closer to the contacts being affected the most, and parts that are more in between will be affected less. The perturbation matrix for this uniform shift looks like

$$W_{\bar{p}\bar{p}} = \frac{\Delta\mu}{2}, \qquad W_{\tilde{p}\tilde{p}} = -\frac{\Delta\mu}{2}, \qquad W_{pq} = 0 \quad \forall \quad p \neq q. \tag{3.4.1a}$$

where the different blocks are defined using the index notation from the previous section. The

resulting $\boldsymbol{V}$ vector now looks like

$$V_{\bar{a}\tilde{i}}^{(e)} = \Delta\mu D_{\tilde{i}\bar{a}}^{(0)}, \qquad V_{\tilde{a}\bar{i}}^{(e)} = \Delta\mu D_{\bar{i}\tilde{a}}^{(0)}, \qquad V_{\bar{a}\bar{i}}^{(e)} = V_{\tilde{a}\tilde{i}}^{(e)} = 0 \qquad (3.4.1b)$$

The other special case is where we couple a specific occupied orbital in a subsystem to a specific virtual orbital in the other subsystem. This looks like the $\boldsymbol{W}$ matrix having some (real or complex) off-diagonal coupling element τ in the b, j and j, b positions, $W_{bj} = W_{jb}^* = \tau$, where b and j are the indices of the virtual and occupied orbitals. The rest of the $\boldsymbol{W}$ matrix is left as zero. No actual perturbation would ever only contain a single element coupling two specific orbitals, but contain many couplings of varying strengths as well as diagonal elements like the ones from the potential shift above. The important thing to note here is that any real perturbation of the form described in eq. (3.3.6) will be a linear combination of different simple coupling perturbations like this, with different orbitals being coupled, as well as different shifts of diagonal elements. This means that together with the fact that the equations for determining the parametrization coefficients and the equations for determining the transport, which are discussed below, are all completely linear in the perturbation operator, the predicted transport will also be a linear combination of the transport from such model perturbations. It is therefore very useful to look at the results from these model perturbations as that gives insight into the components that build up the result in an actual computation. The $\boldsymbol{V}$ vector from such coupling perturbations looks like

$$\boldsymbol{V} = \begin{pmatrix} \boldsymbol{V}^{(e)} \\ -\boldsymbol{V}^{(e)*} \end{pmatrix} \qquad V_\mu^{(e)} = \left(\delta_{ab} D_{ij}^{(0)} - \delta_{ij} D_{ba}^{(0)} \right) \tau \qquad (3.4.2)$$

3.5 Expression for Transport

We want to look at the transported number of electrons from one subsystem to the other. We therefore start by defining the number operator for each of the orbital subspaces as the sum of the number operators for each orbital in the subspace, here for the barred indices, but also identically for the tilded indices,

$$\bar{N} = \sum_{\bar{p}} E_{\bar{p}\bar{p}}. \tag{3.5.1}$$

The average amount of electrons in a subsystem is then the trace of the part of the density matrix corresponding to the main subsystem,

$$\langle \bar{N} \rangle = \sum_{\bar{p}} D_{\bar{p}\bar{p}}, \tag{3.5.2}$$

so we need the density matrix elements of our parameterization. We start with the definition of the one-electron density in the MO basis

$$D_{pq} = \langle E_{pq} \rangle, \tag{3.5.3}$$

then inserting into eq. (2.2.25)

$$D_{pq}^{(0)} = \langle E_{pq} \rangle^{(0)} = \langle 0 | E_{pq} | 0 \rangle, \tag{3.5.4a}$$

$$D_{pq}^{(1)} = \langle E_{pq} \rangle^{(1)} = i \langle 0 | [E_{pq}, \hat{P}^{(1)}] | 0 \rangle, \tag{3.5.4b}$$

we see that the zeroth order density matrix is indeed the density matrix of the zeroth order wavefunction, and we have an expression for the first order correction. We insert for $\hat{P}^{(1)}$ giving

$$[E_{pq}, \hat{P}^{(1)}] = \sum_{ai} \kappa_{ai} [E_{pq}, E_{ai}] + \kappa_{ia} [E_{pq}, E_{ia}] = \sum_{r} \kappa_{qr} E_{pr} - \kappa_{rp} E_{rq}, \tag{3.5.5}$$

which gives the first order correction to the density as

$$D_{pq}^{(1)} = i \sum_{r} \kappa_{qr} D_{pr}^{(0)} - \kappa_{rp} D_{rq}^{(0)}, \tag{3.5.6}$$

with the diagonal elements

$$D_{pp}^{(1)} = i \sum_{q} \kappa_{pq} D_{pq}^{(0)} - (\kappa_{pq} D_{pq}^{(0)})^* = -2 \sum_{q} \text{Im}(\kappa_{pq} D_{pq}^{(0)}) \tag{3.5.7}$$

Again, we are interested in the trace over some subspace changing, which would mean the trace of the first order correction is non-zero. We have the trace of the main subspace as

$$\delta \langle \bar{N} \rangle = \sum_{\bar{p}} D_{\bar{p}\bar{p}}^{(1)}. \tag{3.5.8}$$

$\bar{N}$ now represents the number operator for the main system, with $\tilde{N}$ as the number operator for the other subsystem. The total number operator is the sum of these two $\hat{N} = \bar{N} + \tilde{N}$ with an expectation value $\langle \hat{N} \rangle = 0$, as the total system here is a closed system. Inserting eq. (3.5.7) into eq. (3.5.8) we obtain

$$\delta\langle \bar{N} \rangle = -2 \sum_{\bar{p}p} \mathrm{Im}\left(\kappa_{\bar{p}p} D^{(0)}_{\bar{p}p} \right) = -2 \sum_{\bar{a}i} \mathrm{Im}\left(\kappa_{\bar{a}i} D^{(0)}_{\bar{a}i} \right) - 2 \sum_{\bar{i}a} \mathrm{Im}\left(\kappa_{\bar{i}a} D^{(0)}_{\bar{i}a} \right). \tag{3.5.9}$$

Expanding the indices running over the whole system into the two subspaces ($i = \bar{i}, \tilde{i}$, $a = \bar{a}, \tilde{a}$) we get

$$\begin{aligned}
\delta\langle \bar{N} \rangle = &- 2 \sum_{\bar{a}\bar{i}} \mathrm{Im}\left(\kappa_{\bar{a}\bar{i}} D^{(0)}_{\bar{a}\bar{i}} \right) - 2 \sum_{\bar{i}\bar{a}} \mathrm{Im}\left(\kappa_{\bar{i}\bar{a}} D^{(0)}_{\bar{i}\bar{a}} \right) \\
&- 2 \sum_{\bar{a}\tilde{i}} \mathrm{Im}\left(\kappa_{\bar{a}\tilde{i}} D^{(0)}_{\bar{a}\tilde{i}} \right) - 2 \sum_{\bar{i}\tilde{a}} \mathrm{Im}\left(\kappa_{\bar{i}\tilde{a}} D^{(0)}_{\bar{i}\tilde{a}} \right) \\
= &- 2 \sum_{\bar{a}\tilde{i}} \mathrm{Im}\left(\kappa_{\bar{a}\tilde{i}} D^{(0)}_{\bar{a}\tilde{i}} \right) - 2 \sum_{\bar{i}\tilde{a}} \mathrm{Im}\left(\kappa_{\bar{i}\tilde{a}} D^{(0)}_{\bar{i}\tilde{a}} \right).
\end{aligned} \tag{3.5.10}$$

We will not be looking at any systems where the zeroth order density matrix contains any imaginary parts, so we can simplify this expression to

$$\delta\langle \bar{N} \rangle = -2 \sum_{\bar{a}\tilde{i}} \mathrm{Im}\left(\kappa_{\bar{a}\tilde{i}} \right) D^{(0)}_{\bar{a}\tilde{i}} - 2 \sum_{\bar{i}\tilde{a}} \mathrm{Im}\left(\kappa_{\bar{i}\tilde{a}} \right) D^{(0)}_{\bar{i}\tilde{a}}, \tag{3.5.11}$$

Which is the ultimate equation we use to calculate whether there is transport between two subsystems. In the following section we discuss the implications the form of this equation has on the choice of the ground state wave function model.

3.6 Choice of Ground State Wave Function

The equation we obtained for the transport between subsystems (eq. (3.5.11)) is a sum over the blocks of the zeroth order density coupling the occupied in one system with the virtual in the other and vice versa. For any state where these elements are zero, which means any diagonal (HF) state, or a state where the two subsystems are initially not coupled with each other, will not give rise to any transport in this approximation. These off diagonal density matrix elements are a result of having a state where there is simultaneous contributions from determinants differing by exactly one electron. A simple post-HF ground state method that includes such contributions is the CISD method. It would be useful to have a simplified CISD state only considering a subset of the excited state determinants, for a more transparent and understandable system to run proof of concept calculations on. Our original goal was to implement a CISD method only considering the single and double excited determinants including only excitations between orbitals traditionally considered in transport, e.g. HOMO in one subsystem and LUMO in

the other. However, it turned out to be difficult obtaining correct expressions for the two-electron density matrix elements which as previously discussed are needed in the expression for the elements of the M matrix (eq. (3.3.4)). We therefore switched to use an off-the-shelf implementation of the CISD method from the python module PySCF[55]. It should be noted that for a real world implementation, CISD would not be an optimal choice of ground state calculation. Only the configuration coefficients are variationally optimized, so orbital coefficients are not relaxed and the assumption of the ground state being a solution of the zeroth order equation (eq. (2.2.18)), is not valid. A more suitable ground state method would perhaps be some MCSFC method.

3.7   Implementation

Here we give a brief overview of the proof-of-concept calculations we have implemented for the response theory method described in this chapter. A summary in the form of a flow chart is given in fig. 3.7.1. The systems we have tested have been small/simple enough to be run on a personal computer, so the performance gain of implementing optimized solvers in a high performance quantum computation software like e^T[56] is not needed. We have instead opted for an implementation using the quite new programming language Julia[57] which is a high performance, high level language for scientific computing, allowing for faster and easier development, as well as easy visualization of the results. The implementation consists of a few main steps. Firstly we need the relevant information from the ground state calculation, which includes one- and two-electron integrals and density matrices. As mentioned we are using a CISD implementation from the PySCF[55] python module for the ground state calculation, from which we obtain all the required matrices. Next we determine the localization orbitals as described in section 3.4, which is needed for computation of the V vector in eq. (3.4.1b) and the final computation of transported electron density from eq. (3.5.11). We then need to compute the matrix elements from sections 3.3 and 3.4.1. In the current implementation, the computation of the M is the most time consuming part of the total calculation as it involves a triple nested sum in the calculation of the (ee) block. This results in the computational complexity being proportional to $n_{occ}n_{vir}(n_{occ}+n_{vir})n_{ao}^3$ which is $O(n_{occ}n_{ao}^5)$. In the computation of the V vector we need to chose a value for the parameters we use ($\Delta\mu$ or τ), and since the final result will change linearly with this parameter, we have set this to be 1 a.u, or $1i$ for the imaginary coupling perturbation operator. When we have the M and S matrices and the V vector, we can compute the transported electron density from eq. (3.5.11) for many different values of the dampening parameter γ, only having to solve this equation for each new value of γ. This way we can easily plot the transported electron density as a function of γ.
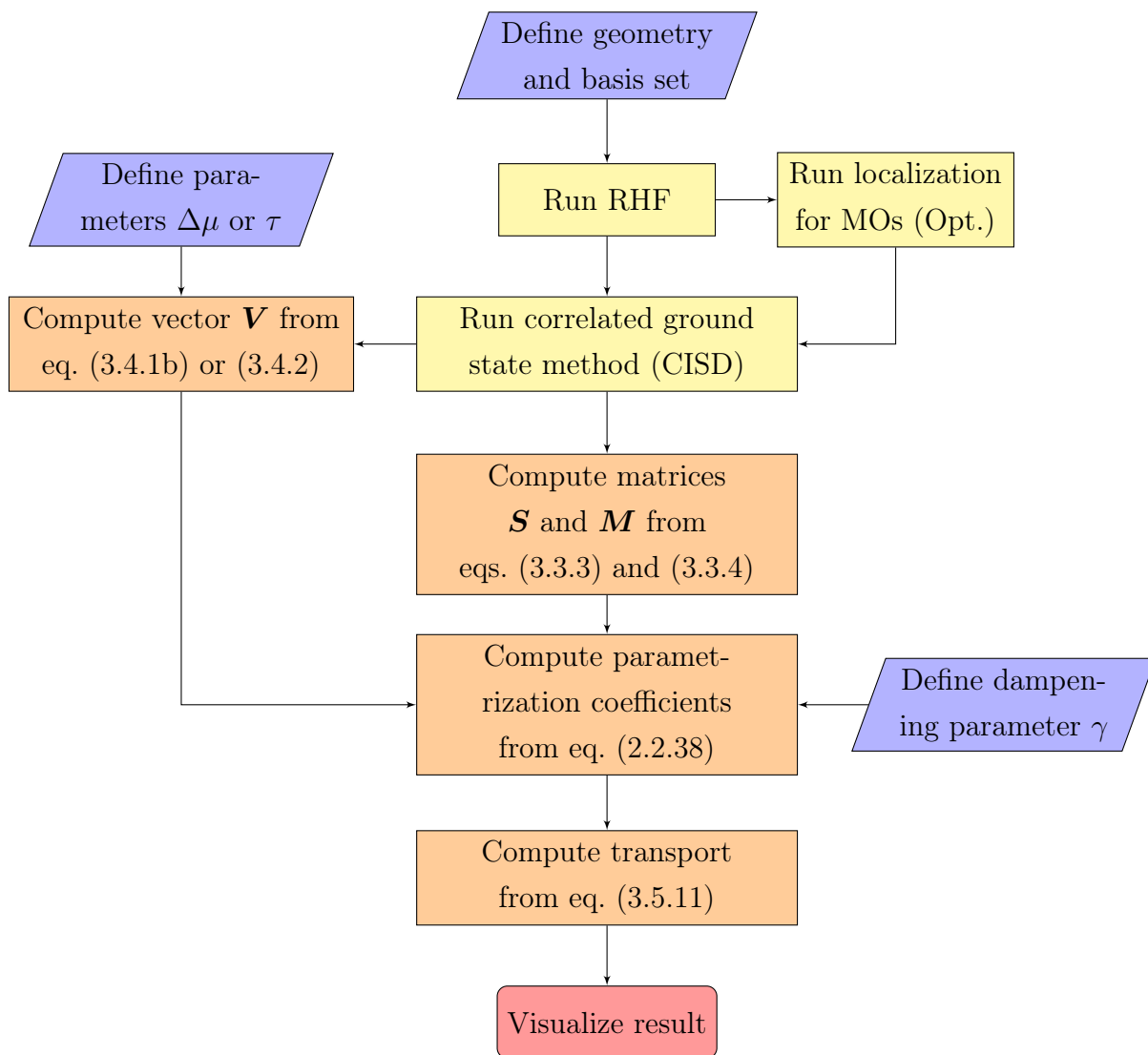
Figure 3.7.1: A brief summary of the steps to compute the electronic transport using the equations described in this chapter. Blue parallelogram nodes represent some parameters we chose as inputs to the computation. Yellow nodes represent a calculation done using the PySCF[55] module. Orange nodes represents a calculation done using equations presented in this thesis implemented in Julia[57].

Chapter 4

Transport from NEGF

NEGF methods are commonly used in physics for describing transport through conducting channels[31]. In this chapter we present a brief overview of the NEGF equations with the purpose of calculating transport in some simple model systems, such that we can compare and draw parallels to the response theory method described in the previous chapter, both in terms of the equations, and the resulting transport.

4.1 Partitioning the System

The reason for wanting to calculate the Green's function is that we can describe a system with some contacts where the effects of the contacts are projected onto the device subspace. This way the problem size is essentially no larger than the size of the device subsystem.
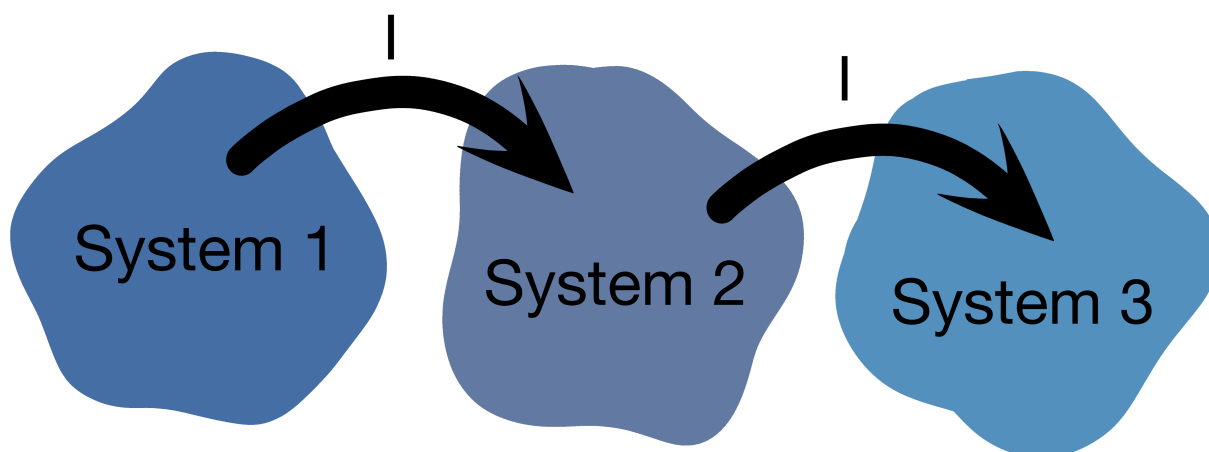

Figure 4.1.1: System partitioned into three subsystems with arrows depicting a current I from system 1 to system 3 through system 2. Credit: Ylva Os

To do this we separate our system into device and contact subspaces. An illustration of the imagined system is given in fig. 4.1.1 where system 1 and 3 are the contacts conected to electron reservoirs, and system 2 is the device. With this separated system we can write the

time independent Schrödinger equation as

$$\begin{pmatrix} \boldsymbol{H}_1 & \boldsymbol{\tau}_1 & \boldsymbol{0} \\ \boldsymbol{\tau}_1^\dagger & \boldsymbol{H}_d & \boldsymbol{\tau}_2^\dagger \\ \boldsymbol{0} & \boldsymbol{\tau}_2 & \boldsymbol{H}_2 \end{pmatrix} \begin{pmatrix} \boldsymbol{\psi}_1 \\ \boldsymbol{\psi}_d \\ \boldsymbol{\psi}_2 \end{pmatrix} = E \begin{pmatrix} \boldsymbol{\psi}_1 \\ \boldsymbol{\psi}_d \\ \boldsymbol{\psi}_2 \end{pmatrix} \qquad (4.1.1)$$

where we here have two contacts, but this can be any number of contact, depending on the system. $\boldsymbol{H}_1$ and $\boldsymbol{H}_2$ are the contact Hamiltonian matrices, and $\boldsymbol{H}_d$ is the device Hamiltonian matrix. $\boldsymbol{\tau}_1$ and $\boldsymbol{\tau}_2$ are matrices describing the coupling between the device and each contact respectively. There is assumed to be no direct coupling between contacts. Good explanations of how to obtain the device and electrode Hamiltonians as well as the coupling Hamiltonians are found in the appendices of[25, 29, 30].

We can now expand eq. (2.3.2) in terms of subspaces

$$\begin{pmatrix} E\boldsymbol{I} - \boldsymbol{H}_1 & -\boldsymbol{\tau}_1 & \boldsymbol{0} \\ -\boldsymbol{\tau}_1^\dagger & E\boldsymbol{I} - \boldsymbol{H}_d & -\boldsymbol{\tau}_2^\dagger \\ \boldsymbol{0} & -\boldsymbol{\tau}_2 & E\boldsymbol{I} - \boldsymbol{H}_2 \end{pmatrix} \begin{pmatrix} \boldsymbol{G}_1 & \boldsymbol{G}_{1d} & \boldsymbol{G}_{12} \\ \boldsymbol{G}_{d1} & \boldsymbol{G}_d & \boldsymbol{G}_{d2} \\ \boldsymbol{G}_{21} & \boldsymbol{G}_{2d} & \boldsymbol{G}_2 \end{pmatrix} = \begin{pmatrix} \boldsymbol{I} & \boldsymbol{0} & \boldsymbol{0} \\ \boldsymbol{0} & \boldsymbol{I} & \boldsymbol{0} \\ \boldsymbol{0} & \boldsymbol{0} & \boldsymbol{I} \end{pmatrix}, \qquad (4.1.2)$$

from which we extract the second column

$$\left(E\boldsymbol{I} - \boldsymbol{H}_1\right)\boldsymbol{G}_{1d} - \boldsymbol{\tau}_1\boldsymbol{G}_d = \boldsymbol{0}, \qquad (4.1.3a)$$

$$-\boldsymbol{\tau}_1^\dagger\boldsymbol{G}_{1d} + \left(E\boldsymbol{I} - \boldsymbol{H}_d\right)\boldsymbol{G}_d - \boldsymbol{\tau}_2^\dagger\boldsymbol{G}_{2d} = \boldsymbol{I}, \qquad (4.1.3b)$$

$$\left(E\boldsymbol{I} - \boldsymbol{H}_2\right)\boldsymbol{G}_{2d} - \boldsymbol{\tau}_2\boldsymbol{G}_d = \boldsymbol{0}. \qquad (4.1.3c)$$

Looking at eqs. (4.1.3a) and (4.1.3c), it is useful to introduce what we refer to as the surface Green's functions for the contacts

$$(E\boldsymbol{I} - \boldsymbol{H}_i)\boldsymbol{g}_i = \boldsymbol{I}, \qquad (4.1.4a)$$

$$\boldsymbol{g}_i = (E\boldsymbol{I} - \boldsymbol{H}_i)^{-1}, \qquad (4.1.4b)$$

which are the green's functions for each of the isolated contacts. This way we can nicely solve for $\boldsymbol{G}_{1d}$ and $\boldsymbol{G}_{2d}$ in terms of $\boldsymbol{G}_d$,

$$\boldsymbol{G}_{1d} = \boldsymbol{g}_1\boldsymbol{\tau}_1\boldsymbol{G}_d, \qquad (4.1.5a)$$

$$\boldsymbol{G}_{2d} = \boldsymbol{g}_2\boldsymbol{\tau}_2\boldsymbol{G}_d. \qquad (4.1.5b)$$

This can then be substituted into eq. (4.1.3b) to obtain

$$-\boldsymbol{\tau}_1^\dagger\boldsymbol{g}_1\boldsymbol{\tau}_1\boldsymbol{G}_d + \left(E\boldsymbol{I} - \boldsymbol{H}_d\right)\boldsymbol{G}_d - \boldsymbol{\tau}_2^\dagger\boldsymbol{g}_2\boldsymbol{\tau}_2\boldsymbol{G}_d = \boldsymbol{I}, \qquad (4.1.6a)$$

$$\left(-\boldsymbol{\tau}_1^\dagger\boldsymbol{g}_1\boldsymbol{\tau}_1 + E\boldsymbol{I} - \boldsymbol{H}_d - \boldsymbol{\tau}_2^\dagger\boldsymbol{g}_2\boldsymbol{\tau}_2\right)\boldsymbol{G}_d = \boldsymbol{I}. \qquad (4.1.6b)$$

We now introduce an important quantity known as the self-energy of the device with respect to each contact

$$\boldsymbol{\Sigma}_i = \boldsymbol{\tau}_i^\dagger \boldsymbol{g}_i \boldsymbol{\tau}_i, \tag{4.1.7a}$$

$$\boldsymbol{\Sigma} = \sum_i \boldsymbol{\Sigma}_i. \tag{4.1.7b}$$

Note that it is in the computation of these self-energy matrices we include the non-zero dampening parameter, η, such that it is the self-energies that include the non-hermiticity of the total Green's function. Specifically, the parameter is included in the computation of the surface Green's functions as

$$\boldsymbol{g}_i = (E\boldsymbol{I} - \boldsymbol{H}_i)^{-1} \rightarrow \boldsymbol{g}_i = (E\boldsymbol{I} + i\eta\boldsymbol{I} - \boldsymbol{H}_i)^{-1} \tag{4.1.8}$$

We can then finally write down the device Green's function neatly as

$$\boldsymbol{G}_d = (E\boldsymbol{I} - \boldsymbol{H}_d - \boldsymbol{\Sigma})^{-1}. \tag{4.1.9}$$

We will only really be considering this device Green's function, so to avoid clutter, from now on when $\boldsymbol{G}$ is written this refers to $\boldsymbol{G}_d$ unless otherwise specified. We see that these self-energies give rise to an effective Hamiltonian

$$\boldsymbol{H}_{eff} = \boldsymbol{H}_d + \boldsymbol{\Sigma} \tag{4.1.10}$$

with $\boldsymbol{G}_d$ being the Green's function of this Hamiltonian. This it not a hermitian Hamiltonian, with all the non hermitian parts included in the self-energy terms. Further we introduce the matrices $\boldsymbol{\Gamma}$ as the anti-hermitian part of the self-energies (similarly to the spectral function in eq. (2.3.6))

$$\boldsymbol{\Gamma}_i = i\left(\boldsymbol{\Sigma}_i - \boldsymbol{\Sigma}_i^\dagger\right), \tag{4.1.11a}$$

$$\boldsymbol{\Gamma} = i\left(\boldsymbol{\Sigma} - \boldsymbol{\Sigma}^\dagger\right) = \sum_i \boldsymbol{\Gamma}_i. \tag{4.1.11b}$$

We can use this to express the spectral function in terms of $\boldsymbol{\Gamma}$ and $\boldsymbol{G}$ as

$$\boldsymbol{A} = \boldsymbol{G}\boldsymbol{\Gamma}\boldsymbol{G}^\dagger. \tag{4.1.12}$$

This is shown by starting with the anti-hermitian part of the inverse Green's function (using $\boldsymbol{G}^{-\dagger}$ as a shorthand for the inverse of $\boldsymbol{G}^\dagger$)

$$i\left(\boldsymbol{G}^{-\dagger} - \boldsymbol{G}^{-1}\right) = i\left(E\boldsymbol{I} - \boldsymbol{H} - \boldsymbol{\Sigma}^\dagger - E\boldsymbol{I} + \boldsymbol{H} + \boldsymbol{\Sigma}\right) = i\left(\boldsymbol{\Sigma} - \boldsymbol{\Sigma}^\dagger\right) = \boldsymbol{\Gamma}, \tag{4.1.13}$$

then multiplying by $\boldsymbol{G}$ from the left and $\boldsymbol{G}^\dagger$ from the right to get

$$i\left(\boldsymbol{G}\boldsymbol{G}^{-\dagger}\boldsymbol{G}^\dagger - \boldsymbol{G}\boldsymbol{G}^{-1}\boldsymbol{G}^\dagger\right) = i(\boldsymbol{G} - \boldsymbol{G}^\dagger) = \boldsymbol{G}\boldsymbol{\Gamma}\boldsymbol{G}^\dagger, \tag{4.1.14}$$

which arrives at the definition of the spectral function.

4.2 Equations for Electrical Current

We start with the time dependent Schrödinger equation for the device part of the system in matrix form perturbed by a constant source term vector $\boldsymbol{s}$

$$i\hbar\frac{\partial}{\partial t}\boldsymbol{\psi} = \boldsymbol{H}\boldsymbol{\psi} + \boldsymbol{\Sigma}\boldsymbol{\psi} + \boldsymbol{s}, \tag{4.2.1}$$

where we have the Green's function matrix

$$\boldsymbol{G} = (E\boldsymbol{I} - \boldsymbol{H} - \boldsymbol{\Sigma})^{-1}, \tag{4.2.2}$$

and the solution to the time independent equation

$$\boldsymbol{\psi} = \boldsymbol{G}\boldsymbol{s}. \tag{4.2.3}$$

We also define what is commonly called the in-scattering function

$$\boldsymbol{\Sigma}^{in} = \boldsymbol{s}\boldsymbol{s}^\dagger. \tag{4.2.4}$$

We want to look at the time derivative of the electron density matrix

$$i\hbar\frac{\partial}{\partial t}\boldsymbol{D} = i\hbar\frac{\partial}{\partial t}\boldsymbol{\psi}\boldsymbol{\psi}^\dagger, \tag{4.2.5}$$

using the product rule to get

$$i\hbar\frac{\partial}{\partial t}\boldsymbol{\psi}\boldsymbol{\psi}^\dagger = \left(i\hbar\frac{\partial}{\partial t}\boldsymbol{\psi}\right)\boldsymbol{\psi}^\dagger + \boldsymbol{\psi}\left(i\hbar\frac{\partial}{\partial t}\boldsymbol{\psi}^\dagger\right). \tag{4.2.6}$$

Now we can use the Schrödinger equation to substitute into

$$\begin{aligned}
&= \left((\boldsymbol{H} + \boldsymbol{\Sigma})\boldsymbol{\psi} + \boldsymbol{s}\right)\boldsymbol{\psi}^\dagger - \boldsymbol{\psi}\left(\boldsymbol{\psi}^\dagger\left(\boldsymbol{H} + \boldsymbol{\Sigma}^\dagger\right) + \boldsymbol{s}^\dagger\right) \\
&= (\boldsymbol{H} + \boldsymbol{\Sigma})\boldsymbol{\psi}\boldsymbol{\psi}^\dagger - \boldsymbol{\psi}\boldsymbol{\psi}^\dagger(\boldsymbol{H} + \boldsymbol{\Sigma}^\dagger) + \boldsymbol{s}\boldsymbol{\psi}^\dagger - \boldsymbol{\psi}\boldsymbol{s}^\dagger,
\end{aligned} \tag{4.2.7}$$

then exchanging $\boldsymbol{\psi}\boldsymbol{\psi}^\dagger$ for $\boldsymbol{D}$, $\boldsymbol{\psi}$ for $\boldsymbol{G}\boldsymbol{s}$ and $\boldsymbol{s}\boldsymbol{s}^\dagger$ for $\boldsymbol{\Sigma}^{in}$ we get

$$\begin{aligned}
&(\boldsymbol{H} + \boldsymbol{\Sigma})\boldsymbol{D} - \boldsymbol{D}(\boldsymbol{H} + \boldsymbol{\Sigma}^\dagger) + \boldsymbol{s}\boldsymbol{s}^\dagger\boldsymbol{G}^\dagger - \boldsymbol{G}\boldsymbol{s}\boldsymbol{s}^\dagger \\
&= \left[\boldsymbol{H}\boldsymbol{D} - (\boldsymbol{H}\boldsymbol{D})^\dagger\right] + \left[\boldsymbol{\Sigma}\boldsymbol{D} - (\boldsymbol{\Sigma}\boldsymbol{D})^\dagger\right] - \left[\boldsymbol{G}\boldsymbol{\Sigma}^{in} - (\boldsymbol{G}\boldsymbol{\Sigma}^{in})^\dagger\right] \\
&= \left[\boldsymbol{\Sigma}\boldsymbol{D} - (\boldsymbol{\Sigma}\boldsymbol{D})^\dagger\right] - \left[\boldsymbol{G}\boldsymbol{\Sigma}^{in} - (\boldsymbol{G}\boldsymbol{\Sigma}^{in})^\dagger\right],
\end{aligned} \tag{4.2.8}$$

where the first term disappears because of hermiticity of both $\boldsymbol{H}$ and $\boldsymbol{D}$. The final equation is then

$$i\hbar\frac{\partial}{\partial t}\boldsymbol{D} = \left[\boldsymbol{\Sigma}\boldsymbol{D} - (\boldsymbol{\Sigma}\boldsymbol{D})^\dagger\right] - \left[\boldsymbol{G}\boldsymbol{\Sigma}^{in} - (\boldsymbol{G}\boldsymbol{\Sigma}^{in})^\dagger\right]. \qquad (4.2.9)$$

We will return to this equation a bit later on to discuss the similarities with damped response theory. Since electrical current is the amount of charge moving, we want to look at the change in the average number of electrons which is the trace of the one-electron density matrix, just as we did for response theory in eq. (3.5.2). Taking the trace of eq. (4.2.9) then gives

$$i\hbar\frac{\partial}{\partial t}N = \text{Tr}\left[\boldsymbol{\Sigma}\boldsymbol{D} - (\boldsymbol{\Sigma}\boldsymbol{D})^\dagger\right] - \text{Tr}\left[\boldsymbol{G}\boldsymbol{\Sigma}^{in} - (\boldsymbol{G}\boldsymbol{\Sigma}^{in})^\dagger\right], \qquad (4.2.10)$$

which using hermiticity of $\boldsymbol{D}$ and $\boldsymbol{\Sigma}^{in}$ and the cyclic property of trace can be easily rearranged into

$$i\hbar\frac{\partial}{\partial t}N = \text{Tr}\left[(\boldsymbol{\Sigma} - \boldsymbol{\Sigma}^\dagger)\boldsymbol{D}\right] - \text{Tr}\left[(\boldsymbol{G} - \boldsymbol{G}^\dagger)\boldsymbol{\Sigma}^{in}\right]. \qquad (4.2.11)$$

Using eqs. (2.3.6) and (4.1.11), we can further simplify to

$$\frac{\partial}{\partial t}N = \frac{1}{\hbar}\text{Tr}[\boldsymbol{A}\boldsymbol{\Sigma}^{in} - \boldsymbol{\Gamma}\boldsymbol{D}], \qquad (4.2.12)$$

and multiplying by the charge per electron, e, we obtain the net current into the system

$$\boldsymbol{I} = \frac{e}{\hbar}\text{Tr}[\boldsymbol{A}\boldsymbol{\Sigma}^{in} - \boldsymbol{\Gamma}\boldsymbol{D}]. \qquad (4.2.13)$$

At steady state, this should be zero (no charge buildup). We can, however, consider the effects of each contact separately[25] to obtain the current into the device from each contact

$$\boldsymbol{I}_i = \frac{e}{\hbar}\text{Tr}[\boldsymbol{A}\boldsymbol{\Sigma}_i^{in} - \boldsymbol{\Gamma}_i\boldsymbol{D}], \qquad (4.2.14)$$

which is the equation we will be using. To do some example calculations we need to be able to calculate the density, $\boldsymbol{D}$, and the in-scattering functions, $\boldsymbol{\Sigma}_i^{in}$, for each of the contacts. We get the density from the total in-scattering function

$$\boldsymbol{D} = \boldsymbol{\psi}\boldsymbol{\psi}^\dagger = \boldsymbol{G}\boldsymbol{s}\boldsymbol{s}^\dagger\boldsymbol{G}^\dagger = \boldsymbol{G}\boldsymbol{\Sigma}^{in}\boldsymbol{G}^\dagger \qquad (4.2.15)$$

and the different in-scattering functions are found from the anti-hermitian parts of the self-energy terms, $\boldsymbol{\Gamma}_i$, and the Fermi energy distribution functions, $f_i(E)$,

$$\boldsymbol{\Sigma}_i^{in} = f_i(E)\boldsymbol{\Gamma}_i. \qquad (4.2.16)$$

For simple molecules we will make these Fermi functions simple Heaviside step functions such that

$$f_i(E) = \begin{cases} 1 & E \leq E_{fi} \\ 0 & E > E_{fi} \end{cases} \qquad (4.2.17)$$

where E_{fi} is the Fermi energy of contact i. For testing simple molecules, we will set the Fermi energy of the contacts equal to the HOMO energy of the contact.

It is important to note that the current in eq. (4.2.14) is a function of the energy level. Evaluated at a single energy this would give the amount of current transported at that energy. To get the total current we need to integrate over all energy

$$I_{\text{tot}} = \int_{\infty}^{\infty} I(E)dE \tag{4.2.18}$$

4.2.1   Note on the comparison with damped response theory

Now that both the damped response theory and NEGF equations have been introduced, we explicitly point out the main similarity in the derivation of the final equations. Earlier from the derivation of the damped Ehrenfest theorem, we obtained eq. (3.2.5) which we wrote in matrix form as eq. (3.2.8), expressing the time derivative of the density matrix. This is very similar to eq. (4.2.9) from the NEGF equations which we can see, writing the two side by side

$$i\hbar\frac{\partial}{\partial t}\boldsymbol{D} = \qquad [\boldsymbol{H}, \boldsymbol{D}] \qquad + \left(\boldsymbol{\Sigma}\boldsymbol{D} - \boldsymbol{D}\boldsymbol{\Sigma}^{\dagger}\right), \tag{4.2.19a}$$

$$i\hbar\frac{\partial}{\partial t}\boldsymbol{D} = -\left(\boldsymbol{G}\boldsymbol{\Sigma}^{in} - (\boldsymbol{G}\boldsymbol{\Sigma}^{in})^{\dagger}\right) + \left(\boldsymbol{\Sigma}\boldsymbol{D} - \boldsymbol{D}\boldsymbol{\Sigma}^{\dagger}\right). \tag{4.2.19b}$$

The $\boldsymbol{\Sigma}$ from the first equation is the part of the Hamiltonian matrix containing any and all non-hermiticity, with $\boldsymbol{H}$ being the remaining hermitian part of the Hamiltonian. In the second equation, $\boldsymbol{\Sigma}$, is the total self-energy matrix which is obtained from the surface Green's functions of the contacts, and serves as a non-hermitian part of the effective Hamiltonian in eq. (4.1.10). If somehow this non-hermitian effective Hamiltonian was the Hamiltonian used in the Ehrenfest theorem, we could equate the remaining part of the equations as

$$[\boldsymbol{H}, \boldsymbol{D}] = -\left(\boldsymbol{G}\boldsymbol{\Sigma}^{in} - (\boldsymbol{G}\boldsymbol{\Sigma}^{in})^{\dagger}\right), \tag{4.2.20}$$

directly connecting the response theory equations to the NEGF equations.

Chapter 5

Results and Discussion

5.1 Results from Response Theory

In this section we present the results from the computations we have done using he response theory based transport equations we have discussed in previous chapters. We have tested the procedure described in section 3.7 for a collection of different simple molecules with different geometries and basis sets. For all molecules we present three different forms of the perturbation operator. The first is the potential difference perturbation described in eq. (3.4.1). The other two are both the coupling perturbation in eq. (3.4.2), one with τ being a real number and the other with it being an imaginary number. For all the molecules we have plotted the transport as a function of the dampening factor. It would in general also be interesting to plot the transport against the perturbation strength, but as can be seen from eqs. (2.2.38), (3.4.1), (3.4.2) and (3.5.11), the relationship between the perturbation and the transport is purely linear, so plotting as a function of the perturbation strength (either $\Delta\mu$ for eq. (3.4.1) or τ for eq. (3.4.2)) would result in straight lines, which are not very interesting. The peak values for the calculated transport with respect to the dampening parameter, γ, is given in table 5.1.1 for all systems tested.

5.1.1 LiH

The first molecule we present here is the lithium hydride (LiH) molecule with a bond length of 2Å using the minimal basis set STO-3G, of which the results can be seen in fig. 5.1.1. The choice of lithium hydride is motivated by it being a small molecule with few electrons and for which oxidation states Li^+ and H^- are plausible. Looking at the movement of charge between the atoms should not be to far from something that could realistically happen. The crystalline form of LiH is ionic and has also experimentally been shown to have interesting optical properties[58].

Coupling

We see in table 5.1.1 that for the real coupling perturbation we get a transport of a whole electron per perturbation strength of one with no dampening. This is the peak we see in

Table 5.1.1: This table contains the peak values for the calculated transport for the different systems we have tested. The system column describes the molecular formula, geometry and basis set of the total system. The subsystem column specifies the atoms we are looking at transport to/from. The $\langle \bar{N}_{\mathrm{HF}} \rangle$ column is the trace of the HF one-electron density matrix, describing the amount of electrons in the orbitals of the subsystem in the HF state. The $\langle \bar{N}_{\mathrm{CISD}} \rangle$ similarly is the same trace for the CISD state, which represents the amount of electrons in the subsystem in the ground state. The transported electron density we calculate is telling how much the amount of electrons differs from this value. The ground state is identical for all three perturbations. The $\delta\langle \bar{N} \rangle$ column is giving the peak amount of transported electrons into the subsystem for a perturbation strength of 1 a.u. The γ column gives the value of the dampening factor, γ, that gives the largest absolute value for the transport in the previous column.

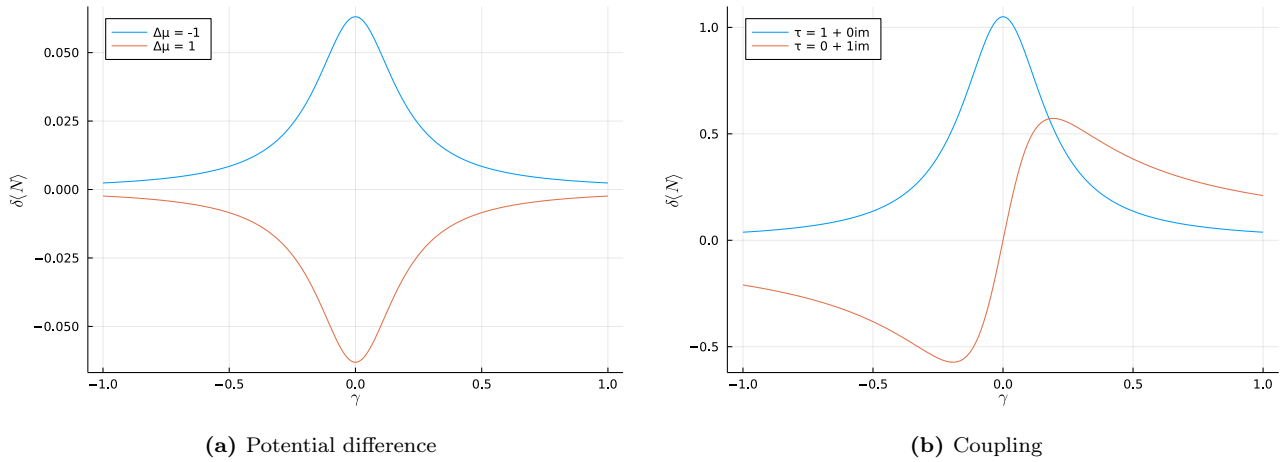| System	Subsystem	Perturbation	$\langle \bar{N}_{\mathrm{HF}} \rangle$	$\langle \bar{N}_{\mathrm{CISD}} \rangle$	$\delta\langle \bar{N} \rangle$	γ
LiH	Li	Real coupling	2.000	1.904	1.050	0.0
STO-3G		Imag coupling			± 0.573	± 0.19
		Potential diff			-0.063	0.0
BeO$_2$	Be	Real coupling	4.000	3.675	-0.200	0.0
L-Shaped		Imag coupling			± 0.341	∓ 0.19
STO-3G		Potential diff			-0.003	0.0
BeO$_2$	Be	Real coupling	4.000	4.010	0.000	0.0
C$_{2\mathrm{V}}$		Imag coupling			0.0	0.0
STO-3G		Potential diff			-0.070	0.0
BeO$_2$	Be	Real coupling	2.000	2.095	0.894	0.0
L-Shaped		Imag coupling			± 0.518	± 0.05
cc-pVDZ		Potential diff			-0.034	0.0

(a) Potential difference

(b) Coupling

Figure 5.1.1: Transport equations from response theory applied on LiH with a bond length of 2Å using the basis set STO-3G. The transport is with respect to the hydrogen atom, meaning a positive value of $\delta\langle N \rangle$ is an increase of electron density around the hydrogen atom. Mind the difference in scale on the y-axis between the two figures.

the blue graph in fig. 5.1.1b. For the imaginary coupling we see a peak of about half of the real coupling peak, with a dampening factor of $\gamma = \pm 0.19$. The coupling perturbation (both real and imaginary) here is coupling the highest occupied (HOMO) and lowest unoccupied (LUMO) canonical molecular orbitals, meaning the indices j and b from eq. (3.4.2) are 2 and 3 respectively. The LUMO orbital here is almost completely localized on the lithium atom, in the sense that 97% of the atomic orbital (AO) contributions are from AOs from lithium. The HOMO orbital however is very delocalized between the two atoms, having about half the AO contributions from each atom. The calculated transport is therefore to be interpreted as electrons moving from being shared between the atoms to belonging to the lithium atom, meaning the actual transported electron density from the hydrogen atom to the lithium atom would be closer to half of what we have shown here.

For the imaginary coupling, we see that the behaviour with respect to the dampening factor is completely different, in mainly two ways. Firstly, when the dampening factor is zero, we observe no transport. This mathematically makes sense, as if we let γ be zero in eq. (2.2.38), we only have $i\boldsymbol{M}^{-1}\boldsymbol{V}$. M is a real matrix, so the product here involves a factor i at the front, and a factor i in the perturbation $\boldsymbol{V}$, making the whole resulting vector $\boldsymbol{\alpha}$ real. Since the transport is a sum over the imaginary parts of this vector (eq. (3.5.11)), it is natural that having no imaginary part results in having no transport. The other difference from the real is that the transport dies of significantly slower as γ tends towards infinity. This is because eq. (2.2.38) essentially behaves like the function $\frac{1}{1+ix}$, where for the real perturbation it is the real part of this that carries through, and for the imaginary perturbation it is the imaginary part. Splitting this into real and imaginary parts we have $\frac{1}{1+ix} = \frac{1}{1+x^2} - i\frac{x}{1+x^2}$, where the real part dies off as $\frac{1}{x^2}$ for large x, and the imaginary part only dies of as $\frac{1}{x}$, explaining the observed result. Of course, the actual equation being a matrix equation, the reality is a lot more complicated, but this gives a quick intuition.

Potential Difference

For the potential difference perturbation we see significantly less transport compared to the coupling perturbations, with a peak value of only 0.063 with no dampening. Mathematically, this is easy to see why. Looking at eqs. (3.4.1b) and (3.4.2), the potential difference perturbation gets contributions from the off-diagonal elements coupling occupied and virtual orbitals in the one-electron density matrix for the ground state, which are inherently small (usually not much larger than 10^{-2} for the systems we have looked at) for post-HF methods such as CISD as we have used here. For such systems the HF state is usually a good approximation for the ground state, with the correlation energy only making up a small portion of the energy. The perturbation operator on the other hand have contributions from elements coupling different occupied with each other, and different virtual with each other. Most notably this includes the diagonal of the occupied block, where elements are close to 2.

5.1.2 BeO$_2$

The next molecule we present here is the beryllium peroxide molecule BeO$_2$ for two different geometries, where we treat the beryllium atom as one system and the oxygen molecule as the other. This serves as a bit larger test system than LiH where we can test the effects of different geometries. The ions Be^{2+} and O$_2{}^{2-}$ are common, so looking at electrons transported between the two ions should not be unreasonable, but the conditions for BeO$_2$ to exist is an active research topic[59]. In all our calculations we work with closed shells, and since the ground state of the oxygen molecule is a triplet state, our ground state calculation will not actually find the true ground state, but rather the excited singlet oxygen state. This will be problematic for quantitative accuracy and will need to be considered, but for these proof of concept calculations, this calculations will still give some insight. In the first geometry the atoms are arranged in an L-shape with the bond length of the oxygen molecule is 1.2 Å, and the distance between the beryllium atom and the closest oxygen atom is 1.6 Å. In the second geometry the atoms are arranged in a C$_{2v}$ symmetry with the bond length of the oxygen molecule still being 1.2 Å, but the distance from the beryllium atom to the center of the oxygen molecule is increased to 1.75 Å. This increase in distance is done because the HF calculation converged to a different minimum if this distance is below about 1.7 Å. In the other solution the HOMO/LUMO orbitals had switched places such that the HOMO orbital now was more localized around oxygen molecule rather than the beryllium atom, in addition to both HOMO and LUMO now being much more delocalized between the two systems. The two geometries are illustrated in fig. 5.1.2.
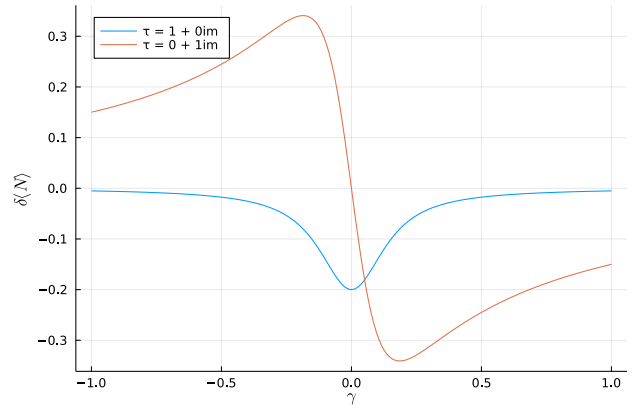

(a) L-shaped geometry.

(b) C$_{2v}$ symmetric geometry.

Figure 5.1.2: The two geometries we have tested for the BeO$_2$ molecule.
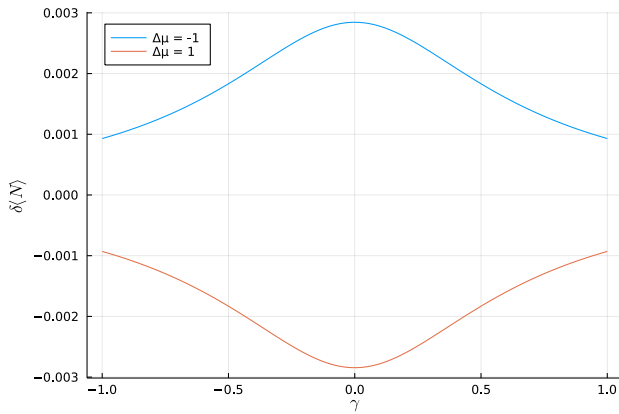
L-shaped

We see that for the L-shaped beryllium peroxide using the STO-3G basis set, the transport is about the same order of magnitude as for the lithium hydride molecule, especially for the potential difference which is almost identical. The coupling perturbation sees three main differences from the lithium hydride molecule, the first one being that the magnitude is about 20-30% of the lithium hydride. The other two differences are that there is a sign change, and that the imaginary coupling gives almost double the transport (at its peak) compared to the real coupling. The sign difference is not something we can draw any meaningful conclusions from here, as the effect of the sign of the off-diagonal elements of such matrices depend on the sign of all the other off-diagonal matrix elements in the calculation (one- and two-electron Hamiltonian matrices, density matrices, etc.), which depend on the sign of the orbital coefficients from the HF calculation. The fact that the imaginary coupling with dampening is larger
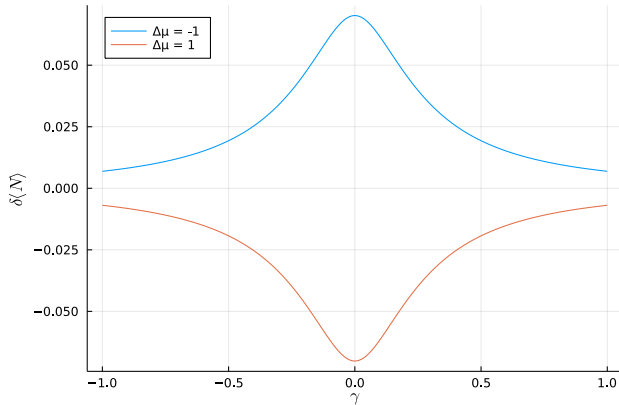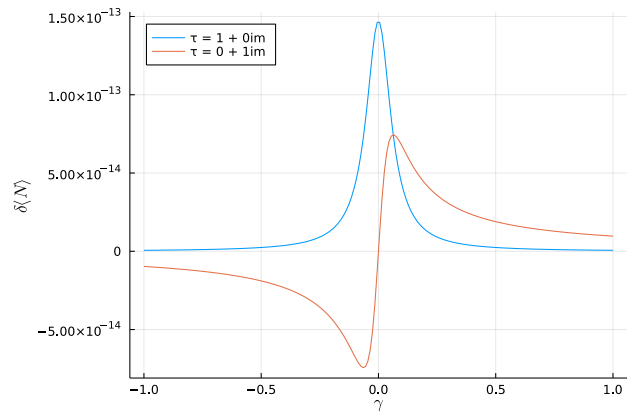
(a) Potential difference perturbation for the L-shaped geometry, using the STO-3G basis set.
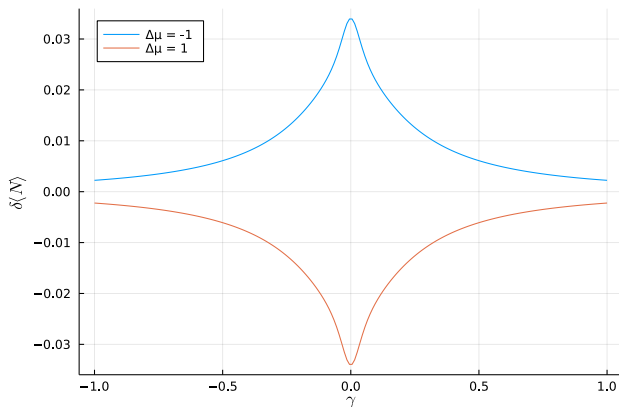
(b) Coupling perturbation for the L-shaped geometry, using the STO-3G basis set.
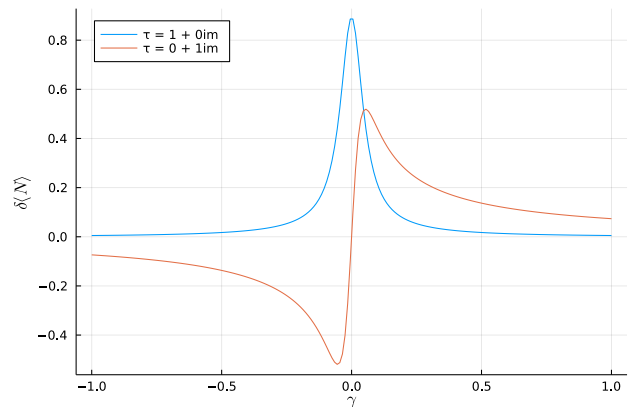
(c) Potential difference perturbation for the C_{2v} geometry, using the STO-3G basis set.

(d) Coupling perturbation for the C_{2v} geometry, using the STO-3G basis set.

(e) Potential difference perturbation for the L-shaped geometry, using the cc-pVDZ basis set.

(f) Coupling perturbation for the L-shaped geometry, using the cc-pVDZ basis set.

Figure 5.1.3: Transport equations from response theory applied on the BeO_2 molecules with the two geometries illustrated in fig. 5.1.2 using the STO-3G basis set for both geometries, and also the cc-pVDZ basis set for the L-shaped geometry. The transport is with respect to the beryllium atom, meaning a positive value of $\delta\langle N \rangle$ is an increase of electron density around the beryllium atom. Mind the difference in scale on the y-axis between the figures.

than the real coupling, however, is interesting as this shows that the dampening factor could be needed to show any significant transport for certain systems. Though it is not easy to say based on the equations why this happens for specific systems.

C_{2v} **Coupling**

In the C_{2v} arranged molecule, we see that for the coupling perturbation, the computation completely breaks down, and the resulting transport is on the order of magnitude of rounding errors. We include this to show that the current implementation is somewhat "fragile" in that small changes to the system, which should not have a large physical effect on the system changes the result completely. Mathematically, it is hard to pinpoint the exact cause of this specific result becoming zero, but it is reasonable to imagine that the symmetry of basis functions resulting in all the terms cancelling out. In the presented results for the coupling perturbation we have chosen a single occupied MO in one subsystem to be coupled to a single virtual MO in the other subsystem. A more physical perturbation would of course include much more complexity, with more couplings between all of the different molecular orbitals as well as diagonal elements. This would help considerably with the inconsistent results we get between the different systems, as the form of the perturbation would actually take into consideration the molecule, rather than just being a model perturbation as we are using here. However, it is very insightful to look at these model perturbations as any actual perturbation, assuming it is represented as a one-electron operator, will just be a linear combination of different such model perturbations. Since all the equations here are completely linear in terms of the perturbation, the resulting transport will also be a linear combination of the transport from different model perturbations. This means that if all the different model perturbations result in zero, or insignificant transport, so will a more realistic perturbation. However, if using a physical perturbation, there should be nothing wrong with the wave function described in eq. (2.2.7), as this is just a (mostly) standard first order damped response theory wave function, so if the predicted transport is not acting properly, the fault should lie elsewhere. This is most likely in our crude way of determining if a MO belongs to which system. For these proof-of-concept calculations, we simply use the AO coefficients as a way of determining whether an orbital belongs to one system or the other, which does not take into account the spacial extent of the orbitals, so orbitals where the majority of the electronic density is actually located between the systems would be set as completely belonging to one of the systems. A better approach might involve looking at the spacial localization of orbitals or the partial charges on the atoms in the different subsystems. The orbital partitioning we have done will however work for proof of concept calculations as these as long as we keep in mind that the results will jump around depending on which subsystem the different orbitals happens to be attributed to.

C_{2v} Potential Difference

The potential difference perturbation on the C_{2v} molecule, however, does produce some none-zero result, but this is rather small, more than an order of magnitude smaller than the corresponding result for the L-shaped geometry. For the potential difference, the problem of the choice of which specific orbitals to couple disappears, as we increase the potential of all orbitals in one subsystem, while decreasing the potential of all the other. The problem of the specific partitioning of the orbitals is however amplified, as now in addition to the calculation of the transport from the perturbed wave function, the perturbation is also determined by the partitioning.

L-Shaped with larger basis set

We have also included the computation on the L-shaped molecule using the larger basis set cc-pVDZ, to show the heavy basis set dependence in the current formulation. The effect of the orbitals being partitioned into the different systems will be potentially much greater now that there exists many more virtual orbitals that are partitioned. We see from table 5.1.1 that the amount of electrons in the Be subsystem is only 2 for the HF state compared to 4 for the STO-3G calculation. From the orbital contributions we see that this is because of the HOMO/LUMO orbitals having "switched places" compared to the STO-3G calculation. The HOMO orbital in the STO-3G calculation has 72% of its AO-contributions from Be AOs, but in the cc-pVDZ, this is only 24%, so by our partitioning scheme, the two electrons in that orbital is now no longer in the Be subsystem and we only have the 2 remaining 1s core electrons. Another important point for having larger basis sets is that the amount of potential coupling elements in the two-electron density matrix for the CISD state is much larger, which could lead to a larger predicted amount of electrons transported, as the equation we have for transport explicitly sum over those elements. For this system we see that this is the case, with a peak value of 0.894 electrons per perturbation strength of 1 for the real coupling perturbation, over 5 times as much as for the STO-3G calculation.

5.1.3 Coupling vs Potential Difference

For all the cases we see that the transport from the potential difference perturbation, although similarly small, all have the same sign. This is in contrast to the coupling perturbation where the sign has no direct meaning, as a coupling has no "direction". When we increase the potential of one atom and reduce the potential of another, we expect that electrons would want to move towards the system with the lower potential, which is what we see in all the example calculations we have done. We see that when we decrease the potential of the system we are looking at, we see an increase in the electronic density in that system, shown by the blue curve in the plots, and since all the equations are linear, flipping the sign of the perturbation flips the sign of the output. It should also not be very surprising that the transport from the potential difference is not very large, as we are looking at a closed system and not an open system

with a coupling to infinite electron reservoirs. The strength of static electric fields needed to move entire electrons between weakly coupled atoms are very large, and would probably not be appropriately described using response theory based on linear perturbation theory. The fact that all of the systems tested, not only gives non-zero answer, but consistently has the expected sign and magnitude, is a good sign for the ability of the method to give answers that make sense for actual systems.

5.2 Results from NEGF

In this section we present the results from the computations we have done using the NEGF equations presented in chapter 4 as well as discussing some comparisons to the results from the response theory method. The test setup is a system of three H_2 molecules with a steady state electrical current flow, and is described in more detail below. It is important to note that the results will not be directly comparable to the results from response theory as the calculated quantity is describing two different phenomena, with the response theory describing a static perturbation, more similar to static electricity, while the NEGF equations describe steady state current flow.

5.2.1 Setting up the System

The system we have used as a test system to show the transport predicted by the NEGF equations is a simplified model system of three H_2 molecules. Each of the H_2 molecules has a bond length of $0.71\,\text{Å}$, as this gives about the minimum energy for a RHF calculation using the STO-3G basis set, which is what we have based the calculations on. This energy surface is found in fig. 5.2.2. The illustration of the test system is found in fig. 5.2.1. To determine the coupling strength between the three H_2 molecules, we have done some calculations on a system of two H_2 molecules. From this we have arbitrarily chosen a coupling strength giving about the same split in molecular orbital energies as we get from the system of two H_2 molecules when the distance between the molecules is about $2.3\,\text{Å}$, as this gave a splitting of the MO-energies of the hydrogen molecules that was not too large and not too small. The couplings of the MO-energies of two H_2 molecules is illustrated in fig. 5.2.3. The split of the two bonding MOs is about 0.055 a.u. at $2.3\,\text{Å}$.
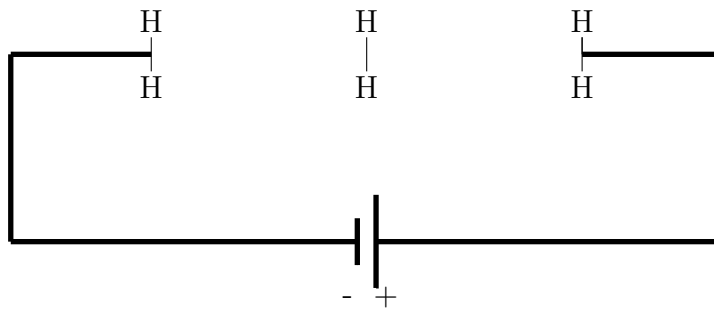

Figure 5.2.1: Illustration of the model system for the NEGF calculations. The bond length of the three hydrogen molecules is $0.71\,\text{Å}$ and the distance between them is $2.3\,\text{Å}$.

To use the NEGF equations as we have presented them, we need to have an expression for the Hamiltonian matrix in eq. (4.1.1). For the device Hamiltonian we will use the Fock matrix of the isolated non-interacting H_2 molecule with a bond length of $0.71\,\text{Å}$ in the MO basis, using the STO-3G basis set. For the contact Hamiltonians we use the same Fock matrix shifted up or down in energy by some electrochemical potential imagined to be applied by some potential
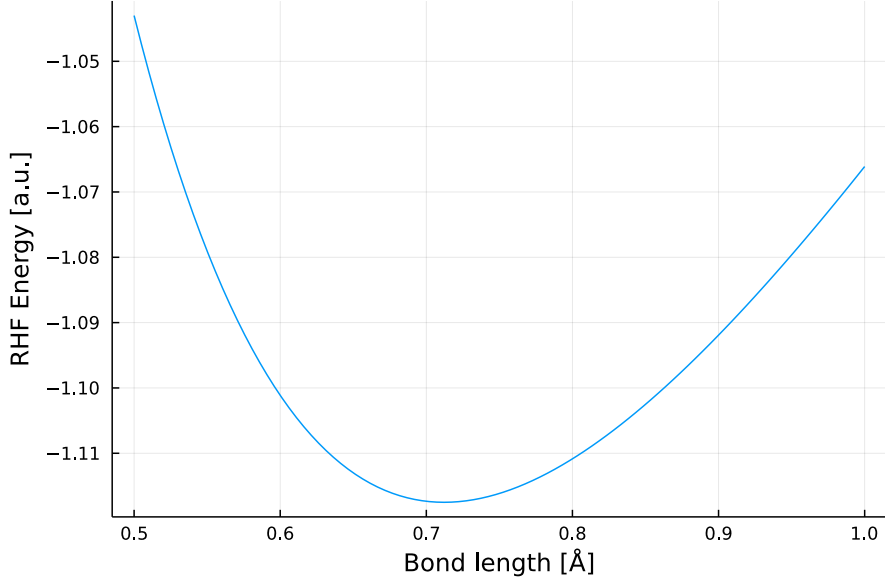
Figure 5.2.2: RHF energy surface of the H_2 molecule using the minimal basis set STO-3G. Calculated using the PySCF python module.

field like illustrated by the battery in fig. 5.2.1. We then have

$$\boldsymbol{H}_d = \boldsymbol{F}_d, \qquad \boldsymbol{H}_1 = \boldsymbol{F}_d + \boldsymbol{I}\frac{\Delta\mu}{2}, \qquad \boldsymbol{H}_2 = \boldsymbol{F}_d - \boldsymbol{I}\frac{\Delta\mu}{2}. \tag{5.2.1}$$

For the coupling Hamiltonian, τ, we need something that gives the resemblance of the MO-split we see from fig. 5.2.3. As a simple model coupling that did this is the uniform 1 matrix,

$$\boldsymbol{\tau} = t \begin{pmatrix} 1 & 1 \\ 1 & 1 \end{pmatrix}, \tag{5.2.2}$$

for some parameter t. This is a very simple coupling which will couple all the orbitals of one H_2 molecule with all the orbitals in the other molecule. In the minimal basis, this is only four couplings, occ-occ, occ-vir, vir-occ and vir-vir, which in reality would be of different strengths. To see that this gives a reasonable effect on the orbitals, we can diagonalize the Fock matrix for two interacting H_2, $\begin{pmatrix} \boldsymbol{F} & \boldsymbol{\tau} \\ \boldsymbol{\tau}^\dagger & \boldsymbol{F} \end{pmatrix}$, and look at the split of the new eigenvalues as a function of the parameter t. This plot is found in fig. 5.2.4. The split with $t = 0.025$ gives a split of about 0.05 a.u. which is the same magnitude as the split of the MOs of the two H_2 system with a distance of 2.3 Å. Now having found this coupling Hamiltonian that emulates the splitting of MOs for a system of two H_2 molecules, we will use this in the system of three H_2 molecules for the NEGF calculations.
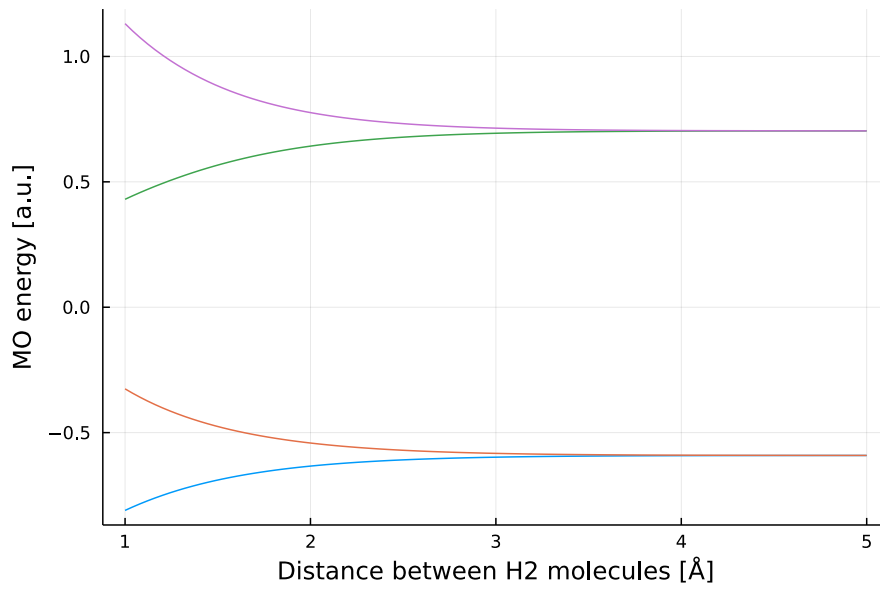
Figure 5.2.3: Plot of the molecular orbital energies of the system of two H_2 molecules with a bond length of 0.71 Å, using the minimal basis set STO-3G. Calculated using the PySCF python module.
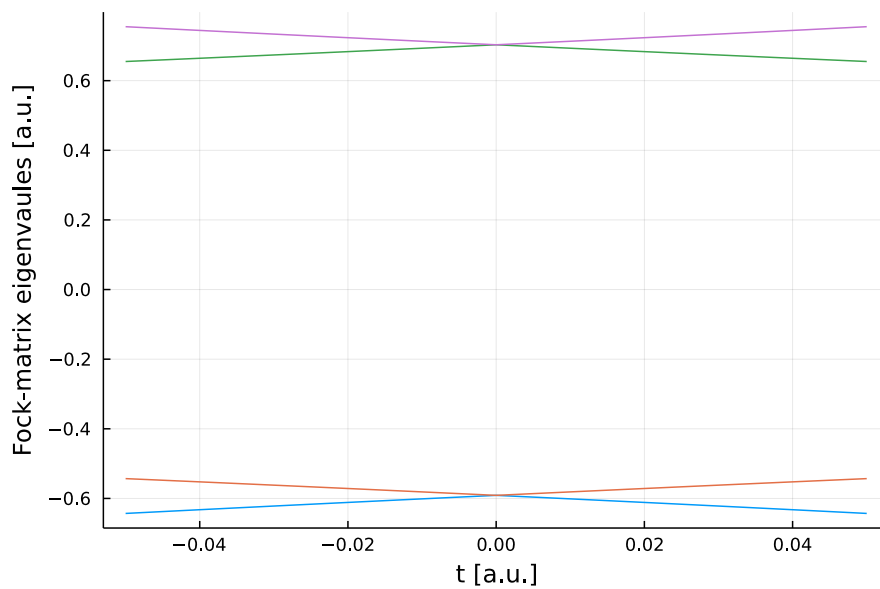

Figure 5.2.4: Plot of eigenvalues of the Fock-matrix of a system of two H_2 molecules coupled by the coupling Hamiltonian in eq. (5.2.2).

5.2.2 Computing Transport from the NEGF Equations

Using the model system we now have set up, we can calculate the steady state current, either as a function of the energy level using eq. (4.2.14), or the total current from eq. (4.2.18). In fig. 5.2.5 we have a plot of the current from eq. (4.2.14), with and without the Fermi energy distribution functions present. We see that when the Fermi distribution functions are present, we have essentially the same plot, but cut off at the Fermi energies. This means that the method only allows for the energy of the transported electrons being between the Fermi energies, such that there exists electrons to take from in one electrode and space to put that electron in the other electrode. We also see from this plot that the current at the two terminals are complete mirror images of each other, meaning in this simple picture that electrons coming into the device carry the same energy as it does leaving the device. Now the energy that we are plotting on the x-axis here is not a parameter of the calculation, but just a variable to be integrated over to get the complete transport. Doing this allows us to plot the transport as a function of the two parameters of the calculation; the dampening factor η, and the potential difference $\Delta\mu$. These plots are found in figs. 5.2.6 and 5.2.7. The total current as a function of both parameters both have a remarkably similar shape to that of the transport predicted by the response theory equations using the imaginary coupling perturbation Hamiltonian (fig. 5.1.3). For the dampening parameter (η, γ), this should not really be surprising, as both in the response theory equation and the NEGF equations the dampening parameter enter the equations in a similar fashion, as an imaginary (almost) diagonal part of a matrix to be inverted, $(\boldsymbol{M} + \hbar\omega\boldsymbol{S} + i\hbar\gamma\boldsymbol{S})^{-1}$ from the response equations (eq. (2.2.35)) and $(E\boldsymbol{I} + i\eta - \boldsymbol{H})^{-1}$ from the NEGF equations (eq. (4.1.8)). Keeping in mind that $E = \hbar\omega$, these equations look very similar.

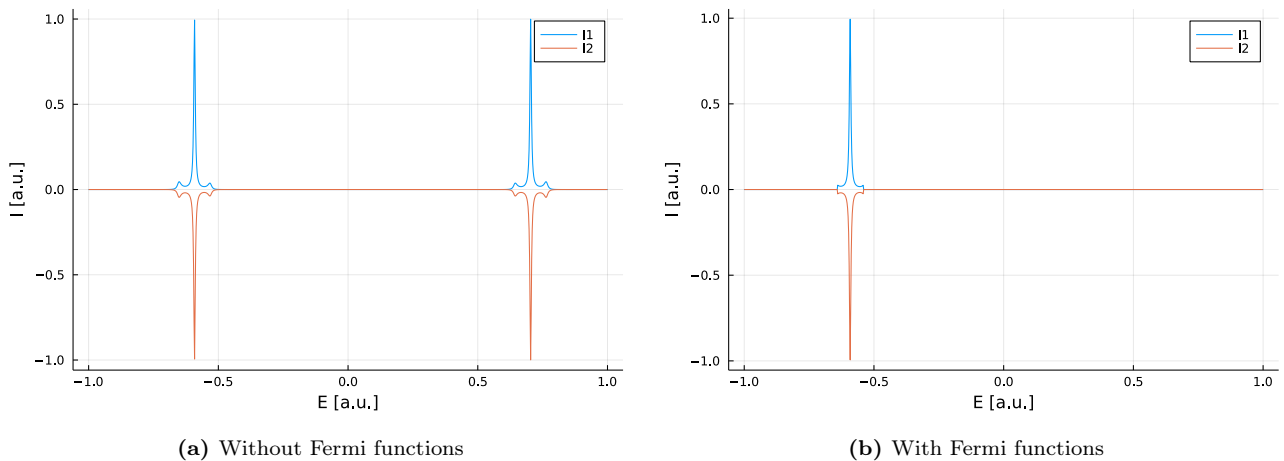(a) Without Fermi functions

(b) With Fermi functions

Figure 5.2.5: The current from eq. (4.2.14) as a function of energy level, with and without the Fermi energy distribution functions enabled, using $\eta = 0.01$ a.u. and $\Delta\mu = 0.1$ a.u.
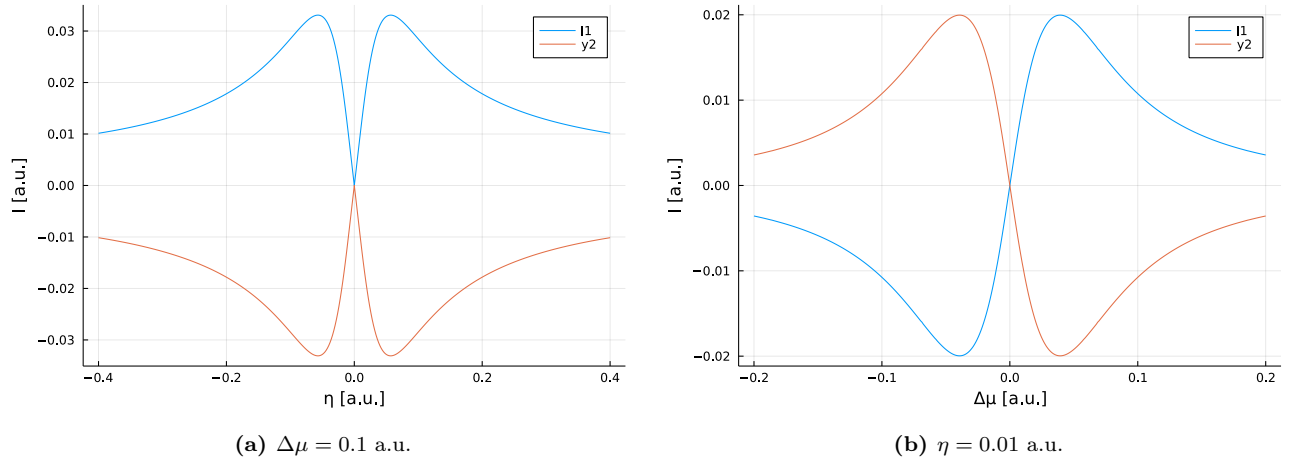
(a) $\Delta\mu = 0.1$ a.u.

(b) $\eta = 0.01$ a.u.

Figure 5.2.6: Total current from eq. (4.2.18) plotted as a function of the dampening factor η and the potential difference $\Delta\mu$ respectively. Both of these are just slices of the 3D plot in fig. 5.2.7.
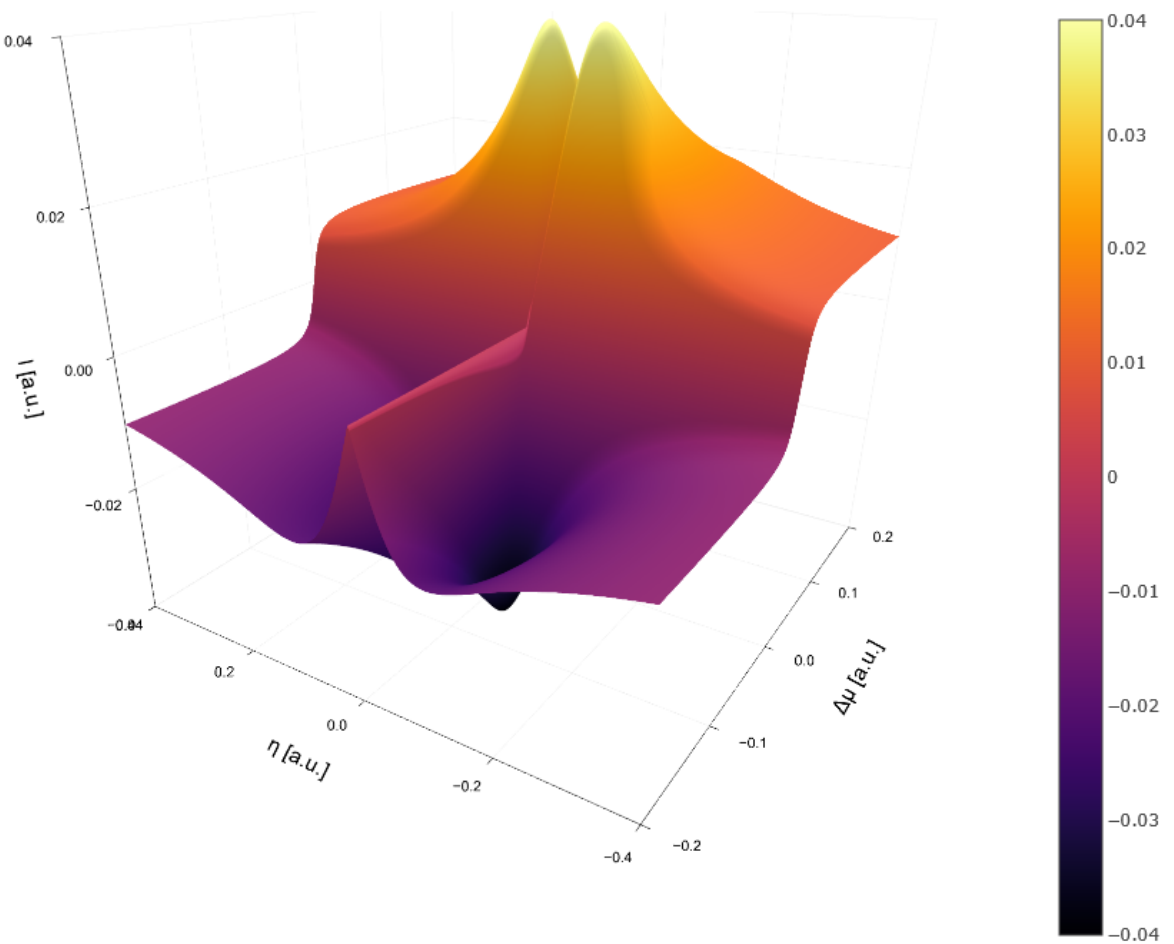

Figure 5.2.7: 3D plot of the total current from eq. (4.2.18) plotted as a function of both the dampening factor η and the potential difference $\Delta\mu$. Interactive version of this plot can be found at `https://folk.ntnu.no/marcustl/master/2d_current.html`

45

Chapter 6

Summary and Conclusions

In this thesis we have presented proof-of-concept calculations using a damped response theory based method for calculating electronic transport. The transport calculated by the method in its current formulation is describing the movement of electrons between parts of a closed system, something resembling a redox reaction. The calculations have been carried out on three test molecules, using small basis sets. The most successful result we obtained was from a LiH molecule with a bond length of $2\,\text{Å}$, where we looked at the transport from the bonding orbital localized between the two atoms to being localized around the lithium atom. This gave a predicted transport of a whole electron per perturbation strength of 1 a.u., illustrating that linear response theory has the potential to give significant results describing electronic transport in sufficiently coupled systems. For the two other systems we tested, both being two different geometries of a BeO_2 molecule, we did not achieve as good, but still promising results. For one of the geometries we got about a third of the transport of the LiH molecule, and for the more symmetric geometry we got virtually zero transport for one of the perturbations we tested. A difference in transport in molecules with different atoms is to be expected, but the fact that a small change in geometry leads to the method breaking down shows that the somewhat arbitrary choices we have made for the partition of the system into different orbital spaces has a huge effect on the results.

The response theory calculations have been done alongside a similar calculation, using a Non Equilibrium Green's Function (NEGF) method to calculate the steady state current through a simple model system of three hydrogen molecules. The purpose of this is to highlight the similarities of the two methods, with the NEGF methods being a pinnacle of modern descriptions of quantum transport. As we have not yet adapted the response theory method to include contacts to electron reservoirs, we can not use the method to describe steady state transport, so the results for the two methods can not be directly compared. Right now the comparison lies more in the mathematical nature of the methods, and for future reference as the method is further developed.

Another fundamental difference between that is important to note, is the difference in ground state calculations. While NEGF methods build upon a HF or DFT ground state, the current simplified formulation of the response theory method would not work for an uncorrelated

ground state model. This makes it more difficult to use the response theory method for simple qualitative calculations, but for any real calculation the ease of incorporating well developed correlated wave function models is a massive strength.

Chapter 7

Further Work

In this chapter we give some ideas on what are the next steps in the further development of response theory based methods for electronic transport. The ultimate goal is to have a rigorous framework for describing different kinds of electronic transport processes in open as well as closed systems, based on response theory. The method we have presented in this thesis is still far from achieving this goal, but we have some ideas for how to continue developing the method. There are two main directions that need development.

First is the incorporation of contacts to electron reservoirs to allow for steady state current, making the method more directly comparable the NEGF methods. This would involve augmenting the current parametrization to allow for a fluctuation of the amount of electrons in the system, making it an open system. This could perhaps be done by adding some types of annihilation/creation to the parametrization operator in eq. (2.2.10) which would add contributions from stated with different numbers of electrons. It would also be useful to further explore the use of non-hermitian perturbations, investigating the connection between NEGF and response theory discussed in eq. (4.2.19).

Second is developing the method towards being quantitatively accurate, using real physically based systems and perturbations. This would involve expanding many of the truncated equations presented in this thesis to higher orders, and comparing results to other proven theoretical models as well as experimental results. When the method is proven for small systems, the goal will be to have an optimized version implemented in some high performance quantum computing software like e^T [56].

Bibliography

[1] Joel Hruska. *14nm, 7nm, 5nm: How low can CMOS go?* URL: https : / / www . extremetech . com / computing / 184946 - 14nm - 7nm - 5nm - how - low - can - cmos - go - it - depends - if - you - ask - the - engineers - or - the - economists (visited on 11/09/2021).

[2] Kevin Morris. *No More Nanometers*. en-US. July 2020. URL: https://www.eejournal. com/article/no-more-nanometers/ (visited on 11/09/2021).

[3] Dexter Johnson. *One-Nanometer Gate Dimensions for Transistors Have Been Achieved*. en. Section: Semiconductors. Oct. 2016. URL: https : / / spectrum . ieee . org / onenanometer - gate - dimensions - for - transistors - have - been - achieved (visited on 11/09/2021).

[4] Dr Ian Cutress. *Intel's Process Roadmap to 2025: with 4nm, 3nm, 20A and 18A?!* URL: https://www.anandtech.com/show/16823/intel-accelerated-offensive-process- roadmap - updates - to - 10nm - 7nm - 4nm - 3nm - 20a - 18a - packaging - foundry - emib - foveros (visited on 11/09/2021).

[5] Gianaurelio Cuniberti, Giorgos Fagas and Klaus Richter. 'Introducing Molecular Electronics: A Brief Overview'. en. In: *Introducing Molecular Electronics*. Ed. by Gianaurelio Cuniberti, Klaus Richter and Giorgos Fagas. Lecture Notes in Physics. Berlin, Heidelberg: Springer, 2005, pp. 1–10. ISBN: 978-3-540-31514-8. DOI: 10.1007/3-540-31514-4_1. URL: https://doi.org/10.1007/3-540-31514-4_1 (visited on 11/09/2021).

[6] Michael Galperin et al. 'Nuclear Coupling and Polarization in Molecular Transport Junctions: Beyond Tunneling to Function'. In: *Science* 319.5866 (Feb. 2008). Publisher: American Association for the Advancement of Science, pp. 1056–1060. DOI: 10.1126/science. 1146556. URL: https://www.science.org/doi/full/10.1126/science.1146556 (visited on 11/09/2021).

[7] Arieh Aviram and Mark A. Ratner. 'Molecular rectifiers'. en. In: *Chemical Physics Letters* 29.2 (Nov. 1974), pp. 277–283. ISSN: 0009-2614. DOI: 10.1016/0009-2614(74)85031-1. URL: https://www.sciencedirect.com/science/article/pii/0009261474850311 (visited on 02/08/2021).

[8] Michael Thoss and Ferdinand Evers. 'Perspective: Theory of quantum transport in molecular junctions'. In: *The Journal of Chemical Physics* 148.3 (Jan. 2018). Publisher: American Institute of Physics, p. 030901. ISSN: 0021-9606. DOI: `10.1063/1.5003306`. URL: `https://aip.scitation.org/doi/full/10.1063/1.5003306` (visited on 02/08/2021).

[9] Sriharsha V. Aradhya and Latha Venkataraman. 'Single-molecule junctions beyond electronic transport'. en. In: *Nature Nanotechnology* 8.6 (June 2013), pp. 399–410. ISSN: 1748-3395. DOI: `10.1038/nnano.2013.91`. URL: `https://www.nature.com/articles/nnano.2013.91` (visited on 06/08/2021).

[10] Diana Dulić et al. 'One-Way Optoelectronic Switching of Photochromic Molecules on Gold'. In: *Physical Review Letters* 91.20 (Nov. 2003). Publisher: American Physical Society, p. 207402. DOI: `10.1103/PhysRevLett.91.207402`. URL: `https://link.aps.org/doi/10.1103/PhysRevLett.91.207402` (visited on 07/09/2021).

[11] Nicolás Agrait, Alfredo Levy Yeyati and Jan M. van Ruitenbeek. 'Quantum properties of atomic-sized conductors'. en. In: *Physics Reports* 377.2 (Apr. 2003), pp. 81–279. ISSN: 0370-1573. DOI: `10.1016/S0370-1573(02)00633-6`. URL: `https://www.sciencedirect.com/science/article/pii/S0370157302006336` (visited on 11/09/2021).

[12] Rama Venkatasubramanian et al. 'Thin-film thermoelectric devices with high room-temperature figures of merit'. en. In: *Nature* 413.6856 (Oct. 2001). Bandiera_abtest: a Cg_type: Nature Research Journals Number: 6856 Primary_atype: Research Publisher: Nature Publishing Group, pp. 597–602. ISSN: 1476-4687. DOI: `10.1038/35098012`. URL: `https://www.nature.com/articles/35098012` (visited on 11/09/2021).

[13] Michael Galperin and Abraham Nitzan. 'Molecular optoelectronics: the interaction of molecular conduction junctions with light'. en. In: *Physical Chemistry Chemical Physics* 14.26 (2012). Publisher: Royal Society of Chemistry, pp. 9421–9438. DOI: `10.1039/C2CP40636E`. URL: `https://pubs.rsc.org/en/content/articlelanding/2012/cp/c2cp40636e` (visited on 11/08/2021).

[14] Enrique Burzurí et al. 'Franck–Condon Blockade in a Single-Molecule Transistor'. In: *Nano Letters* 14.6 (June 2014). Publisher: American Chemical Society, pp. 3191–3196. ISSN: 1530-6984. DOI: `10.1021/nl500524w`. URL: `https://doi.org/10.1021/nl500524w` (visited on 07/09/2021).

[15] Renaud Leturcq et al. 'Franck–Condon blockade in suspended carbon nanotube quantum dots'. en. In: *Nature Physics* 5.5 (May 2009). Bandiera_abtest: a Cg_type: Nature Research Journals Number: 5 Primary_atype: Research Publisher: Nature Publishing Group, pp. 327–331. ISSN: 1745-2481. DOI: `10.1038/nphys1234`. URL: `https://www.nature.com/articles/nphys1234` (visited on 07/09/2021).

[16] H. B. Heersche et al. 'Electron Transport through Single Mn12 Molecular Magnets'. In: *Physical Review Letters* 96.20 (May 2006). Publisher: American Physical Society, p. 206801. DOI: 10.1103/PhysRevLett.96.206801. URL: https://link.aps.org/doi/10.1103/PhysRevLett.96.206801 (visited on 07/09/2021).

[17] Stefan Ballmann et al. 'Experimental Evidence for Quantum Interference and Vibrationally Induced Decoherence in Single-Molecule Junctions'. In: *Physical Review Letters* 109.5 (July 2012). Publisher: American Physical Society, p. 056801. DOI: 10.1103/PhysRevLett.109.056801. URL: https://link.aps.org/doi/10.1103/PhysRevLett.109.056801 (visited on 11/09/2021).

[18] H. Vazquez et al. 'Probing the conductance superposition law in single-molecule circuits with parallel paths'. en. In: *Nature Nanotechnology* 7.10 (Oct. 2012), pp. 663–667. ISSN: 1748-3395. DOI: 10.1038/nnano.2012.147. URL: https://www.nature.com/articles/nnano.2012.147 (visited on 11/09/2021).

[19] Manuel Natali and Silvia Giordani. 'Molecular switches as photocontrollable "smart" receptors'. en. In: *Chemical Society Reviews* 41.10 (2012). Publisher: Royal Society of Chemistry, pp. 4010–4029. DOI: 10.1039/C2CS35015G. URL: https://pubs.rsc.org/en/content/articlelanding/2012/cs/c2cs35015g (visited on 07/09/2021).

[20] Gerasimos M. Tsivgoulis and Jean-Marie Lehn. 'Photonic Molecular Devices: Reversibly Photoswitchable Fluorophores for Nondestructive Readout for Optical Memory'. In: *Angewandte Chemie International Edition in English* 34.10 (1995), pp. 1119–1122. ISSN: 1521-3773. DOI: 10.1002/anie.199511191. URL: https://onlinelibrary.wiley.com/doi/abs/10.1002/anie.199511191 (visited on 07/09/2021).

[21] Giacomo E. M. Crisenza and Paolo Melchiorre. 'Chemistry glows green with photoredox catalysis'. en. In: *Nature Communications* 11.1 (Feb. 2020), p. 803. ISSN: 2041-1723. DOI: 10.1038/s41467-019-13887-8. URL: https://www.nature.com/articles/s41467-019-13887-8 (visited on 02/08/2021).

[22] Kirsten Zeitler. 'Photoredox Catalysis with Visible Light'. In: *Angewandte Chemie International Edition* 48.52 (2009), pp. 9785–9789. ISSN: 1521-3773. DOI: 10.1002/anie.200904056. URL: https://onlinelibrary.wiley.com/doi/abs/10.1002/anie.200904056 (visited on 07/09/2021).

[23] Jun Xuan and Wen-Jing Xiao. 'Visible-Light Photoredox Catalysis'. en. In: *Angewandte Chemie International Edition* 51.28 (2012), pp. 6828–6838. ISSN: 1521-3773. DOI: 10.1002/anie.201200223. URL: https://onlinelibrary.wiley.com/doi/abs/10.1002/anie.201200223 (visited on 07/09/2021).

[24] Thomas Bondo Pedersen. 'Introduction to Response Theory'. en. In: *Handbook of Computational Chemistry*. Ed. by Jerzy Leszczynski. Dordrecht: Springer Netherlands, 2016, pp. 1–26. ISBN: 978-94-007-6169-8. DOI: 10.1007/978-94-007-6169-8_5-2. URL: https://doi.org/10.1007/978-94-007-6169-8_5-2 (visited on 04/08/2021).

[25] Supriyo Datta. 'NEGF Method'. In: *Lessons from Nanoelectronics*. Vol. Volume 5. Lessons from Nanoscience: A Lecture Notes Series. World Scientific, Mar. 2017, pp. 43–64. ISBN: 978-981-322-460-5. DOI: `10.1142/9789813224629_0003`. URL: `https://www.worldscientific.com/doi/abs/10.1142/9789813224629_0003` (visited on 07/07/2021).

[26] Sreekant V. J. Narumanchi, Jayathi Y. Murthy and Cristina H. Amon. 'Boltzmann transport equation-based thermal modeling approaches for hotspots in microelectronics'. en. In: *Heat and Mass Transfer* 42.6 (Apr. 2006), pp. 478–491. ISSN: 1432-1181. DOI: `10.1007/s00231-005-0645-6`. URL: `https://doi.org/10.1007/s00231-005-0645-6` (visited on 07/08/2021).

[27] A. J. H. McGaughey and M. Kaviany. 'Quantitative validation of the Boltzmann transport equation phonon thermal conductivity model under the single-mode relaxation time approximation'. In: *Physical Review B* 69.9 (Mar. 2004). Publisher: American Physical Society, p. 094303. DOI: `10.1103/PhysRevB.69.094303`. URL: `https://link.aps.org/doi/10.1103/PhysRevB.69.094303` (visited on 07/08/2021).

[28] Wu Li. 'Electrical transport limited by electron-phonon coupling from Boltzmann transport equation: An ab initio study of Si, Al, and MoS2'. In: *Physical Review B* 92.7 (Aug. 2015). Publisher: American Physical Society, p. 075405. DOI: `10.1103/PhysRevB.92.075405`. URL: `https://link.aps.org/doi/10.1103/PhysRevB.92.075405` (visited on 07/08/2021).

[29] Supriyo Datta. *Electronic Transport in Mesoscopic Systems*. Cambridge Studies in Semiconductor Physics and Microelectronic Engineering. Cambridge: Cambridge University Press, 1995. ISBN: 978-0-521-59943-6. DOI: `10.1017/CBO9780511805776`. URL: `https://www.cambridge.org/core/books/electronic-transport-in-mesoscopic-systems/1E55DEF5978AA7B843FF70337C220D8B` (visited on 07/07/2021).

[30] Supriyo Datta. *Electronic Transport in Mesoscopic Systems*. en. Cambridge University Press, May 1997. ISBN: 978-0-521-59943-6.

[31] Jeff Schueler. 'Green's Functions and Their Applications to Quantum Mechanics'. en. In: . (June 2011), p. 15.

[32] Alicia Rae Welden. *Finite-Temperature Green's Function Methods for ab-initio Quantum Chemistry: Thermodynamics, Spectra, and Quantum Embedding*. 2018. URL: `https://deepblue.lib.umich.edu/handle/2027.42/146034` (visited on 23/01/2020).

[33] Kristian S. Thygesen and Angel Rubio. 'Nonequilibrium GW approach to quantum transport in nano-scale contacts'. In: *The Journal of Chemical Physics* 126.9 (Mar. 2007). Publisher: American Institute of Physics, p. 091101. ISSN: 0021-9606. DOI: `10.1063/1.2565690`. URL: `https://aip.scitation.org/doi/full/10.1063/1.2565690` (visited on 07/09/2021).

[34] Kristian S. Thygesen and Angel Rubio. 'Conserving GW scheme for nonequilibrium quantum transport in molecular contacts'. In: *Physical Review B* 77.11 (Mar. 2008). Publisher: American Physical Society, p. 115333. DOI: 10.1103/PhysRevB.77.115333. URL: https://link.aps.org/doi/10.1103/PhysRevB.77.115333 (visited on 02/08/2021).

[35] X. Wang et al. 'Electronic correlation in nanoscale junctions: Comparison of the GW approximation to a numerically exact solution of the single-impurity Anderson model'. In: *Physical Review B* 77.4 (Jan. 2008). Publisher: American Physical Society, p. 045119. DOI: 10.1103/PhysRevB.77.045119. URL: https://link.aps.org/doi/10.1103/PhysRevB.77.045119 (visited on 07/09/2021).

[36] F. Aryasetiawan and O. Gunnarsson. 'Electronic Structure of NiO in the GW Approximation'. In: *Physical Review Letters* 74.16 (Apr. 1995). Publisher: American Physical Society, pp. 3221–3224. DOI: 10.1103/PhysRevLett.74.3221. URL: https://link.aps.org/doi/10.1103/PhysRevLett.74.3221 (visited on 07/08/2021).

[37] M. Strange et al. 'Self-consistent GW calculations of electronic transport in thiol- and amine-linked molecular junctions'. In: *Physical Review B* 83.11 (Mar. 2011). Publisher: American Physical Society, p. 115108. DOI: 10.1103/PhysRevB.83.115108. URL: https://link.aps.org/doi/10.1103/PhysRevB.83.115108 (visited on 07/09/2021).

[38] Janet L. Dodds, Roy McWeeny and Andrzej J. Sadlej. 'Self-consistent perturbation theory'. In: *Molecular Physics* 34.6 (Dec. 1977), pp. 1779–1791. ISSN: 0026-8976. DOI: 10.1080/00268977700102961. URL: https://doi.org/10.1080/00268977700102961 (visited on 07/09/2021).

[39] Jeppe Olsen et al. 'Quadratic Response Functions in a Second-Order Polarization Propagator Framework'. In: *The Journal of Physical Chemistry A* 109.50 (Dec. 2005). Publisher: American Chemical Society, pp. 11618–11628. ISSN: 1089-5639. DOI: 10.1021/jp054207w. URL: https://doi.org/10.1021/jp054207w (visited on 05/07/2021).

[40] H. S. Radt and R. P. Hurst. 'Magnetic Quadrupole Polarizability of Closed-Shell Atoms'. In: *Physical Review A* 2.3 (Sept. 1970). Publisher: American Physical Society, pp. 696–706. DOI: 10.1103/PhysRevA.2.696. URL: https://link.aps.org/doi/10.1103/PhysRevA.2.696 (visited on 07/09/2021).

[41] Stefan Grimme. 'Calculation of frequency dependent optical rotation using density functional response theory'. en. In: *Chemical Physics Letters* 339.5 (May 2001), pp. 380–388. ISSN: 0009-2614. DOI: 10.1016/S0009-2614(01)00356-6. URL: https://www.sciencedirect.com/science/article/pii/S0009261401003566 (visited on 07/09/2021).

[42] Dieter Cremer. 'Møller–Plesset perturbation theory: from small molecule methods to methods for thousands of atoms'. en. In: *WIREs Computational Molecular Science* 1.4 (2011), pp. 509–530. ISSN: 1759-0884. DOI: 10.1002/wcms.58. URL: https://onlinelibrary.wiley.com/doi/abs/10.1002/wcms.58 (visited on 05/08/2021).

[43] A. Ilderton. 'Note on the conjectured breakdown of QED perturbation theory in strong fields'. In: *Physical Review D* 99.8 (Apr. 2019). Publisher: American Physical Society, p. 085002. DOI: `10.1103/PhysRevD.99.085002`. URL: `https://link.aps.org/doi/10.1103/PhysRevD.99.085002` (visited on 05/08/2021).

[44] R. G. Woolley and B. T. Sutcliffe. 'Molecular structure and the born—Oppenheimer approximation'. en. In: *Chemical Physics Letters* 45.2 (Jan. 1977), pp. 393–398. ISSN: 0009-2614. DOI: `10.1016/0009-2614(77)80298-4`. URL: `https://www.sciencedirect.com/science/article/pii/0009261477802984` (visited on 16/08/2021).

[45] J. C. Slater. 'A Simplification of the Hartree-Fock Method'. In: *Physical Review* 81.3 (Feb. 1951). Publisher: American Physical Society, pp. 385–390. DOI: `10.1103/PhysRev.81.385`. URL: `https://link.aps.org/doi/10.1103/PhysRev.81.385` (visited on 16/08/2021).

[46] Anna I. Krylov. 'Spin-flip configuration interaction: an electronic structure model that is both variational and size-consistent'. en. In: *Chemical Physics Letters* 350.5 (Dec. 2001), pp. 522–530. ISSN: 0009-2614. DOI: `10.1016/S0009-2614(01)01316-1`. URL: `https://www.sciencedirect.com/science/article/pii/S0009261401013161` (visited on 19/08/2021).

[47] Stefan Grimme, Christian Mück-Lichtenfeld and Jens Antony. 'Analysis of non-covalent interactions in (bio)organic molecules using orbital-partitioned localized MP2'. en. In: *Physical Chemistry Chemical Physics* 10.23 (2008). Publisher: Royal Society of Chemistry, pp. 3327–3334. DOI: `10.1039/B803508C`. URL: `https://pubs.rsc.org/en/content/articlelanding/2008/cp/b803508c` (visited on 19/08/2021).

[48] Galina M. Chaban and R. Benny Gerber. 'Anharmonic vibrational spectroscopy calculations with electronic structure potentials: comparison of MP2 and DFT for organic molecules'. en. In: *Theoretical Chemistry Accounts* 120.1 (May 2008), pp. 273–279. ISSN: 1432-2234. DOI: `10.1007/s00214-007-0299-1`. URL: `https://doi.org/10.1007/s00214-007-0299-1` (visited on 19/08/2021).

[49] R. F. Bishop. 'An overview of coupled cluster theory and its applications in physics'. en. In: *Theoretica chimica acta* 80.2 (Mar. 1991), pp. 95–148. ISSN: 1432-2234. DOI: `10.1007/BF01119617`. URL: `https://doi.org/10.1007/BF01119617` (visited on 19/08/2021).

[50] Tor S. Haugland et al. 'Coupled Cluster Theory for Molecular Polaritons: Changing Ground and Excited States'. In: *Physical Review X* 10.4 (Dec. 2020). Publisher: American Physical Society, p. 041043. DOI: `10.1103/PhysRevX.10.041043`. URL: `https://link.aps.org/doi/10.1103/PhysRevX.10.041043` (visited on 19/08/2021).

[51] Jeppe Olsen and Poul Jo/rgensen. 'Linear and nonlinear response functions for an exact state and for an MCSCF state'. In: *The Journal of Chemical Physics* 82.7 (Apr. 1985). Publisher: American Institute of Physics, pp. 3235–3264. ISSN: 0021-9606. DOI: `10.1063/`

1.448223. URL: https://aip.scitation.org/doi/abs/10.1063/1.448223 (visited on 05/07/2021).

[52] Patrick Norman et al. 'Nonlinear response theory with relaxation: The first-order hyperpolarizability'. In: *The Journal of Chemical Physics* 123.19 (Nov. 2005). Publisher: American Institute of Physics, p. 194103. ISSN: 0021-9606. DOI: 10.1063/1.2107627. URL: https://aip.scitation.org/doi/full/10.1063/1.2107627 (visited on 05/07/2021).

[53] M. Paulsson. 'Non Equilibrium Green's Functions for Dummies: Introduction to the One Particle NEGF equations'. In: *arXiv:cond-mat/0210519* (Jan. 2006). arXiv: cond-mat/0210519. URL: http://arxiv.org/abs/cond-mat/0210519 (visited on 07/07/2021).

[54] Ida-Marie Høyvik and Poul Jørgensen. 'Characterization and Generation of Local Occupied and Virtual Hartree–Fock Orbitals'. In: *Chemical Reviews* 116.5 (Mar. 2016). Publisher: American Chemical Society, pp. 3306–3327. ISSN: 0009-2665. DOI: 10.1021/acs.chemrev.5b00492. URL: https://doi.org/10.1021/acs.chemrev.5b00492 (visited on 13/09/2021).

[55] Qiming Sun et al. 'PySCF: the Python-based simulations of chemistry framework'. en. In: *WIREs Computational Molecular Science* 8.1 (2018), e1340. ISSN: 1759-0884. DOI: 10.1002/wcms.1340. URL: https://onlinelibrary.wiley.com/doi/abs/10.1002/wcms.1340 (visited on 16/08/2021).

[56] Sarai D. Folkestad et al. 'eT 1.0: An open source electronic structure program with emphasis on coupled cluster and multilevel methods'. In: *The Journal of Chemical Physics* 152.18 (May 2020). Publisher: American Institute of Physics, p. 184103. ISSN: 0021-9606. DOI: 10.1063/5.0004713. URL: https://aip.scitation.org/doi/full/10.1063/5.0004713 (visited on 12/09/2021).

[57] Jeff Bezanson et al. 'Julia: A Fresh Approach to Numerical Computing'. In: *SIAM Review* 59.1 (Jan. 2017). Publisher: Society for Industrial and Applied Mathematics, pp. 65–98. ISSN: 0036-1445. DOI: 10.1137/141000671. URL: https://epubs.siam.org/doi/abs/10.1137/141000671 (visited on 16/08/2021).

[58] F. E. Pretzel et al. 'Properties of lithium hydride I. Single crystals'. en. In: *Journal of Physics and Chemistry of Solids* 16.1 (Nov. 1960), pp. 10–20. ISSN: 0022-3697. DOI: 10.1016/0022-3697(60)90064-0. URL: https://www.sciencedirect.com/science/article/pii/0022369760900640 (visited on 12/09/2021).

[59] Shoutao Zhang et al. 'Pressure-Induced Stable Beryllium Peroxide'. In: *Inorganic Chemistry* 56.9 (May 2017). Publisher: American Chemical Society, pp. 5233–5238. ISSN: 0020-1669. DOI: 10.1021/acs.inorgchem.7b00365. URL: https://doi.org/10.1021/acs.inorgchem.7b00365 (visited on 12/09/2021).

Appendix A

Computing Response Theory Matrix Elements

We want to obtain expressions for the matrix elements in eq. (2.2.32).

We can partition $\boldsymbol{\Lambda}$ into two blocks

$$\boldsymbol{\Lambda} = \begin{pmatrix} \boldsymbol{\Lambda}^{(e)} \\ \boldsymbol{\Lambda}^{(d)} \end{pmatrix}, \tag{A.0.1}$$

where the first is all the excitation (e) operators, and the second are all the de-excitation operators (d). This way we can nicely express the matrices as block matrices

$$\boldsymbol{S} = \begin{pmatrix} \boldsymbol{S}^{(ee)} & \boldsymbol{S}^{(ed)} \\ \boldsymbol{S}^{(de)} & \boldsymbol{S}^{(dd)} \end{pmatrix}, \qquad \boldsymbol{M} = \begin{pmatrix} \boldsymbol{M}^{(ee)} & \boldsymbol{M}^{(ed)} \\ \boldsymbol{M}^{(de)} & \boldsymbol{M}^{(dd)} \end{pmatrix}, \qquad \boldsymbol{V} = \begin{pmatrix} \boldsymbol{V}^{(e)} \\ \boldsymbol{V}^{(d)} \end{pmatrix}. \tag{A.0.2}$$

Throughout this appendix, the indices μ, ν will be used for indexing into $\boldsymbol{\Lambda}$, otherwise normal MO-indices i, j, a, b will be used. This way an index μ or ν will correspond to a particular excitation or de-excitation index pair ai or ia.

A.1 The $\boldsymbol{S}$ matrix

We start with the first block of the $\boldsymbol{S}$ matrix

$$S_{\mu\nu}^{(ee)} = \langle 0|[\Lambda_\mu^{(e)\dagger}, \Lambda_\nu^{(e)}]|0\rangle = \langle 0|[E_{ai}, E_{jb}]|0\rangle =$$
$$\delta_{ij}\langle 0|E_{ab}|0\rangle - \delta_{ab}\langle 0|E_{ji}|0\rangle = \delta_{ij}D_{ab}^{(0)} - \delta_{ab}D_{ji}^{(0)}. \tag{A.1.1a}$$

Then the next diagonal block

$$S_{\mu\nu}^{(dd)} = \langle 0|[E_{ia}, E_{bj}]|0\rangle = \delta_{ab}D_{ij}^{(0)} - \delta_{ij}D_{ba}^{(0)}, \tag{A.1.1b}$$

where if we assume the zeroth order density to be real, it is symmetric and we have

$$\boldsymbol{S}^{(dd)} = -\boldsymbol{S}^{(ee)}. \tag{A.1.1c}$$

The two off diagonal blocks are easily seen to be zero as the commutator

$$[E_{ai}, E_{bj}] = 0 \tag{A.1.1d}$$

is zero. We can then write $\boldsymbol{S}$ simply as

$$\boldsymbol{S} = \begin{pmatrix} \boldsymbol{S}^{(ee)} & 0 \\ 0 & -\boldsymbol{S}^{(ee)}, \end{pmatrix} \tag{A.1.1e}$$

with

$$S_{\mu\nu}^{(ee)} = \delta_{ij} D_{ab}^{(0)} - \delta_{ab} D_{ji}^{(0)}. \tag{A.1.1f}$$

A.2 The $\boldsymbol{M}$ matrix

The expression for $\boldsymbol{M}$ will be different depending on what we let the zeroth order Hamiltonian ($\hat{H}^{(0)}$) be. Here we let the zeroth order Hamiltonian be the standard full unperturbed Hamiltonian

$$\hat{H}^{(0)} = h_{nuc} + \sum_{pq} h_{pq} E_{pq} + \frac{1}{2} \sum_{pqrs} g_{pqrs} e_{pqrs}, \tag{A.2.1}$$

since that is the Hamiltonian we have used to find the reference CISD state.

We start with the first block

$$M_{\mu\nu}^{(ee)} = \langle 0 | [[E_{ia}, \hat{H}^{(0)}], E_{bj}] | 0 \rangle. \tag{A.2.2a}$$

Inner commutator:

$$[E_{ia}, \hat{H}^{(0)}] = \sum_{p} h_{ap} E_{ip} - h_{pi} E_{pa} + \sum_{pqr} g_{pqar} e_{pqir} - g_{pqri} e_{pqra} \tag{A.2.2b}$$

60

Outer commutator:

$$[[E_{ia}, \hat{H}^{(0)}], E_{bj}] =$$

$$\sum_p h_{ap}[E_{ip}, E_{bj}] - h_{pi}[E_{pa}, E_{bj}] + \sum_{pqr} g_{pqar}[e_{pqir}, E_{bj}] - g_{pqri}[e_{pqra}, E_{bj}] =$$

$$\sum_p h_{ap}(\delta_{pb}E_{ij} - \delta_{ij}E_{bp}) - h_{pi}(\delta_{ab}E_{pj} - \delta_{pj}E_{ba}) +$$

$$\sum_{pqr} \begin{array}{l} (g_{pqar}(\delta_{rb}e_{pqij} - \delta_{ij}e_{pqbr} + \delta_{qb}e_{pjir} - \delta_{pj}e_{bqir}) - \\ g_{pqri}(\delta_{ab}e_{pqrj} - \delta_{rj}e_{pqba} + \delta_{qb}e_{pjra} - \delta_{pj}e_{bqra})) \end{array} = \quad \text{(A.2.2c)}$$

$$h_{ab}E_{ij} + h_{ji}E_{ba} - \delta_{ij}\sum_p h_{ap}E_{bp} - \delta_{ab}\sum_p h_{pi}E_{pj} +$$

$$\sum_{pq} \begin{array}{l} (g_{pqab}e_{pqij} + g_{pbaq}e_{pjiq} - g_{jpaq}e_{bpiq} \;\; + \\ g_{pqji}e_{pqba} - g_{pbqi}e_{pjqa} + g_{jpqi}e_{bpqa}) \end{array}$$

$$-\delta_{ij}\sum_{pqr} g_{pqar}e_{pqbr} - \delta_{ab}\sum_{pqr} g_{pqri}e_{pqrj}$$

Inserting into the expectation value to get

$$M_{\mu\nu}^{(ee)} = h_{ab}D_{ij}^{(0)} + h_{ji}D_{ba}^{(0)} + \sum_{pq} \begin{array}{l}\left(g_{pqab}d_{pqij}^{(0)} + g_{pbaq}d_{pjiq}^{(0)} - g_{jpaq}d_{bpiq}^{(0)} \;\; + \right.\\ \left. g_{pqji}d_{pqba}^{(0)} - g_{pbqi}d_{pjqa}^{(0)} + g_{jpqi}d_{bpqa}^{(0)} \right)\end{array} \quad \text{(A.2.2d)}$$

$$-\delta_{ij}\sum_p h_{ap}D_{bp}^{(0)} - \delta_{ab}\sum_p h_{pi}D_{pj}^{(0)} - \delta_{ij}\sum_{pqr} g_{pqar}d_{pqbr}^{(0)} - \delta_{ab}\sum_{pqr} g_{pqri}d_{pqrj}^{(0)}.$$

No cancellations were made, so we can now get the rest of the blocks simply by swapping i with a and j with b.
First the other diagonal block

$$M_{\mu\nu}^{(dd)} = h_{ij}D_{ab}^{(0)} + h_{ba}D_{ji}^{(0)} + \sum_{pq} \begin{array}{l}\left(g_{pqij}d_{pqab}^{(0)} + g_{pjiq}d_{pbaq}^{(0)} - g_{bpiq}d_{jpaq}^{(0)} \;\; + \right.\\ \left. g_{pqba}d_{pqji}^{(0)} - g_{pjqa}d_{pbqi}^{(0)} + g_{bpqa}d_{jpqi}^{(0)} \right)\end{array} \quad \text{(A.2.3)}$$

$$-\delta_{ab}\sum_p h_{ip}D_{jp}^{(0)} - \delta_{ij}\sum_p h_{pa}D_{pb}^{(0)} - \delta_{ab}\sum_{pqr} g_{pqir}d_{pqjr}^{(0)} - \delta_{ij}\sum_{pqr} g_{pqra}d_{pqrb}^{(0)}.$$

Next in the off diagonal blocks, the second line will become zero due to $\delta_{ib} = \delta_{ja} = 0$.

$$M_{\mu\nu}^{(de)} = h_{ib}D_{aj}^{(0)} + h_{ja}D_{bi}^{(0)} +$$
$$\sum_{pq} \left(g_{pqib}d_{pqaj}^{(0)} + g_{pbiq}d_{pjaq}^{(0)} - g_{jpiq}d_{bpaq}^{(0)} + g_{pqja}d_{pqbi}^{(0)} - g_{pbqa}d_{pjqi}^{(0)} + g_{jpqa}d_{bpqi}^{(0)} \right) \quad \text{(A.2.4a)}$$

$$M_{\mu\nu}^{(ed)} = h_{aj}D_{ib}^{(0)} + h_{bi}D_{ja}^{(0)} +$$
$$\sum_{pq} \left(g_{pqaj}d_{pqib}^{(0)} + g_{pjaq}d_{pbiq}^{(0)} - g_{bpaq}d_{jpiq}^{(0)} + g_{pqbi}d_{pqja}^{(0)} - g_{pjqi}d_{pbqa}^{(0)} + g_{bpqi}d_{jpqa}^{(0)} \right) \quad \text{(A.2.4b)}$$

61

Notes on Hermiticity

$$M_{\mu\nu}^{(dd)} = \langle 0|[[E_{ai}, \hat{H}^{(0)}], E_{jb}]|0\rangle = \langle 0|[[E_{ia}, \hat{H}^{(0)}], E_{bj}]|0\rangle^\dagger = M_{\mu\nu}^{(ee)\dagger} \tag{A.2.5}$$

$$M_{\mu\nu}^{(ed)} = \langle 0|[[E_{ia}, \hat{H}^{(0)}], E_{jb}]|0\rangle = \langle 0|[[E_{ai}, \hat{H}^{(0)}], E_{bj}]|0\rangle^\dagger = M_{\mu\nu}^{(de)\dagger} \tag{A.2.6}$$

$$\begin{aligned} M_{\mu\nu}^\dagger &= \langle 0|[[\Lambda_\mu^\dagger, \hat{H}^{(0)}], \Lambda_\nu]^\dagger|0\rangle = \langle 0|[\Lambda_\nu^\dagger, [\Lambda_\mu^\dagger, \hat{H}^{(0)}]^\dagger]|0\rangle \\ &= \langle 0|[\Lambda_\nu^\dagger, [\hat{H}^{(0)}, \Lambda_\mu]]|0\rangle = \langle 0|[[\Lambda_\mu, \hat{H}^{(0)}], \Lambda_\nu^\dagger]|0\rangle \end{aligned} \tag{A.2.7}$$

A.3 The **V** vector

To get an expression for **V** we need to chose what the form of the perturbation Hamiltonian $H^{(1)}$. Here we will chose this to be some one-electron operator given by

$$\hat{H}^{(1)} = \sum_{pq} V_{pq} E_{pq}, \tag{A.3.1}$$

where V_{pq} makes up some hermitian matrix describing the perturbation. We insert this into the expression for V

$$\begin{aligned} V_\mu^{(e)} &= \langle 0|[E_{ia}, \hat{H}^{(1)}]|0\rangle = \sum_{pq} V_{pq}\langle 0|[E_{ia}, E_{pq}]|0\rangle \\ &= \sum_{pq} V_{pq}(\delta_{ap} D_{iq}^{(0)} - \delta_{iq} D_{pa}^{(0)}) = \sum_p V_{ap} D_{ip}^{(0)} - V_{pi} D_{pa}^{(0)} \end{aligned} \tag{A.3.2}$$

then $V^{(d)}$ is easily found to be $-V^{(e)\dagger}$ as

$$V_\mu^{(d)} = \langle 0|[E_{ai}, \hat{H}^{(1)}]|0\rangle = -\langle 0|[E_{ia}, \hat{H}^{(1)}]|0\rangle^\dagger = -V_\mu^{(e)\dagger}. \tag{A.3.3}$$

Special case for diagonal V (Potential Difference)

$$V_{pq} = \delta_{pq} V_{pp} \tag{A.3.4}$$

$$V_\mu^{(e)} = \sum_p V_{ap} D_{ip}^{(0)} - V_{pi} D_{pa}^{(0)} = (V_{aa} - V_{ii}) D_{ia}^{(0)} \tag{A.3.5}$$

Special case for single off diagonal V (Increased coupling)

$$V_{bj} = V_{jb}^\dagger = \tau \tag{A.3.6}$$

$$V_\mu^{(e)} = \sum_p V_{ap} D_{ip}^{(0)} - V_{pi} D_{pa}^{(0)} = \left(\delta_{ab} D_{ij}^{(0)} - \delta_{ij} D_{ba}^{(0)}\right) \tau \tag{A.3.7}$$